LUND UNIVERSITY

Three-dimensional T1 quantification techniques for assessment of cartilage quality using dGEMRIC

Siversson, Carl

2011

Three-dimensional T_1 quantification techniques for assessment of cartilage quality using dGEMRIC

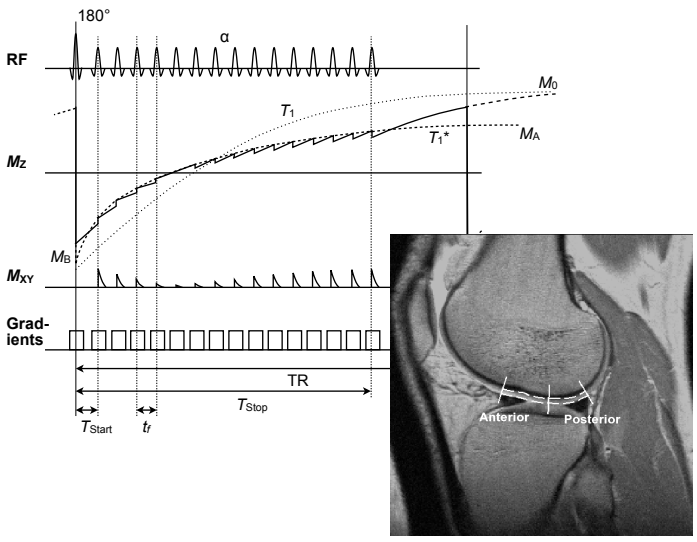

Carl Siversson

Medical Radiation Physics
Department of Clinical Sciences, Malmö
Faculty of Medicine, Lund University
2011

Three-dimensional T_1 quantification techniques for assessment of cartilage quality using dGEMRIC

LUND
UNIVERSITY

Carl Siversson

Cover: Diagram showing the magnetization evolution during one repetition of a Look-Locker pulse sequence (see section 4.2) together with an MRI image showing typical regions of interest in the knee (see section 2.4).

Lund University, Faculty of Medicine Doctoral Dissertation Series 2011:74
ISBN 978-91-86871-24-6
ISSN 1652-8220

Printed in Sweden by Media-Tryck, Lund University
Lund 2011

Abstract

Osteoarthritis (OA) is a common chronic disease and one of the major global causes for functional disabilities. The disease is characterized by loss and degradation of cartilage, commonly affecting the knees and hips. Delayed gadolinium-enhanced MRI of cartilage (dGEMRIC) is a previously presented method for identification of early OA using magnetic resonance imaging (MRI). By quantifying the T_1 parameter in the cartilage after distribution of a contrast agent, a measure of the glycosaminoglycan (GAG) content is retrieved, which in turn is known to be decreased at early stages of OA.

In this thesis a series of three-dimensional (3D) T_1 quantification methods have been developed and evaluated for use in dGEMRIC. Traditionally, such sequences have not been widely adopted for this purpose and in this work it has been shown that the main obstacles are related to B_1 variations within the volume.

As part of the work a 3D Look-Locker (3D-LL) T_1 quantification pulse sequence have been created. In addition, new methods were developed for correction of B_1 inhomogeneities and slab profile flip angle variations in the 3D-LL data. From *in vivo* and phantom measurements the methods were shown to be reliable, with T_1 results that agreed very well to gold standard two-dimensional inversion recovery (2D-IR).

A 3D variable flip angle (3D-VFA) T_1 quantification sequence in combination with a B_1 mapping sequence was also investigated. The results with and without B_1 correction was studied *in vivo* and in phantoms. It was concluded that 3D-VFA should always be used with B_1 correction, especially at higher field strengths

In addition, two dedicated clinical studies were set up, to both verify the usability of the developed methods and to explore new dGEMRIC applications. In one of these studies, the repeatability of successive dGEMRIC measurements for each of the T_1 quantification methods was investigated for a group of subjects at risk of developing OA. 2D-IR and 3D-LL performed equally well, while 3D-VFA (without B_1 correction) was inferior. Repeatability was shown to be similar to previously reported results in healthy subjects.

The other of these studies was a time-response study, using 3D-LL, to explore the feasibility of performing dGEMRIC in the meniscus. It was concluded that the temporal contrast uptake in the meniscus follows that of the articular cartilage and that differences can be seen between vascular and avascular parts of the meniscus.

The overall conclusion of this work is that 3D T_1 quantification in dGEMRIC is feasible and should allow for both new and improved means of diagnostics.

Popular scientific summary in swedish

Artros är en av de vanligaste kroniska sjukdomarna och en av de främsta orsakerna till funktionshinder för människor världen över. Artros angriper ofta knä- och höftlederna och bryter ner det brosk som finns där. För den som drabbats av artros tar förloppet ofta många år, med successivt ökande smärtor och rörelsesvårigheter. Ofta upptäcks dessutom inte sjukdomen förrän i ett sent stadie, när processen inte längre går att förhindra. I många fall är den enda utvägen att den skadade leden, efter en tids sjukdom, opereras bort och ersätts med en protes.

Under de senaste åren har vår forskargrupp, tillsammans med andra grupper, utvecklat en metod för att upptäcka artros i ett så tidigt skede att sjukdomsförloppet förhoppningsvis kan fördröjas med många år. Metoden benämns dGEMRIC (delayed gadolinium-enhanced MRI of cartilage) och bygger på att man ger patienten ett ofarligt kontrastmedel som tas upp av brosket i en mängd som beror av artrosgraden. Genom att med en magnetkamera därefter mäta den så kallade T_1 parametern i brosket, kan koncentrationen av kontrastmedel i brosket bestämmas och därmed graden av artros uppskattas.

En nackdel med dGEMRIC metoden hittills har varit att man med magnetkamerorna bara har kunnat mäta T_1 i tvådimensionella snittbilder genom brosket, vilket har inneburit att det har varit svårt att få en uppfattning om artrosgraden i hela leden. Det är detta problem som denna avhandling syftar till att lösa, genom att ta fram nya tredimensionella volumetriska T_1-mätningsmetoder som gör att magnetkameran kan undersöka allt brosk i leden samtidigt.

Som en del i detta arbete har egna pulssekvenser till magnetkamerorna utvecklats samt analysverktyg tagits fram som genom matematiska algoritmer beräknar broskkvaliteten utifrån magnetkamerabilderna. För att utvärdera de nya mätmetoderna har flera studier genomförts, både på friska och artrossjuka personer. Resultaten visar att de nya tredimensionella metoderna fungerar, vilket kommer att göra det möjligt att följa sjukdomen på sätt som tidigare inte varit möjligt.

Analys- och visualiseringsmetoderna kommer nu att vidareutvecklas samt paketeras så att de blir enkla att använda. Bland annat håller ett datorprogram på att tas fram där man enkelt kan se hur kvaliteten på brosket varierar på olika ställen i leden. Framförallt riktar sig detta till läkare, men det ska också kunna användas för att utvärdera funktionen hos framtida artrosläkemedel. Därigenom är förhoppningen att detta kommer att bli ett viktigt verktyg inom brosk- och leddiagnostik.

Abbreviations

2D	two-dimensional
2D-IR	2D inversion recovery
3D	three-dimensional
3D-LL	3D Look-Locker
3D-VFA	3D variable flip angle
BMI	body mass index
dGEMRIC	delayed gadolinium-enhanced MRI of cartilage
FID	free induction decay
GAG	glycosaminoglycan
gagCEST	glycosaminoglycan chemical exchange saturation transfer
$Gd\text{-}DTPA^{2-}$	gadolinium diethylenetriaminepentaacetic acid (Magnevist)
MR	magnetic resonance
MRI	magnetic resonance imaging
NMR	nuclear magnetic resonance
OA	osteoarthritis
PD	proton density
RF	radio frequency
ROI	region of interest

List of Symbols

B_0	static magnetic field
B_1	magnetic field induced by RF pulse
K	factor representing the accuracy of a 180° inversion pulse
k_x	the readout direction of k-space
k_y	the phase encoding direction of k-space
k_z	the slab direction of k-space
M	net magnetization
M_0	initial magnetization
M_x	magnetization in x-direction
M_y	magnetization in y-direction
M_z	magnetization in z-direction
M_{xy}	magnetization in xy-plane
Na	sodium
T_1	longitudinal relaxation time
T_1^*	apparent longitudinal relaxation time
T_{1pre}	T_1 value prior to contrast agent administration
T_{1Gd}	T_1 value after contrast agent administration
$T_{1\rho}$	T_1 value in the rotating frame
T_2	transverse relaxation time
T_2^*	apparent transverse relaxation time
TE	echo time
TI	inversion time
TR	repetition time
TD	delay time
ν_0	Larmor frequency
α	Excitation pulse flip angle
γ	gyromagnetic ratio

Original papers

This thesis is based on the following papers, referred to in the text by their Roman numerals.

I. **Local Flip Angle Correction for Improved Volume T1-Quantification in Three-Dimensional dGEMRIC Using the Look-Locker Technique**, Carl Siversson, Carl-Johan Tiderius, Leif E Dahlberg and Jonas Svensson, Journal of Magnetic Resonance Imaging, 30(4):834-41 (2009)

II. **Repeatability of T1-Quantification in dGEMRIC for Three Different Acquisition Techniques: Two-Dimensional Inversion Recovery, Three-Dimensional Look-Locker and Three-Dimensional Variable Flip Angle**, Carl Siversson, Carl-Johan Tiderius, Paul Neuman, Leif E Dahlberg and Jonas Svensson, Journal of Magnetic Resonance Imaging, 31(5):1203-9 (2010)

III. **Effects of B1 Inhomogeneity Correction for 3D Variable Flip Angle T1 Measurements in Hip dGEMRIC at 3T and 1.5T**, Carl Siversson, Jenny Chan, Carl-Johan Tiderius, Tallal Mamisch, Vladimir Jellus, Jonas Svensson and Young-Jo Kim, Accepted in Magnetic Resonance in Medicine (2011)

IV. **In Vivo Transport of Gd-DTPA^{2-} into Human Meniscus and Cartilage Assessed with dGEMRIC**, Ulf Sigurdsson, Carl Siversson, Carl-Johan Tiderius, Eveliina Lammentausta, Jonas Svensson and Leif E Dahlberg, Manuscript (2011)

Preliminary reports

The following preliminary reports were given at international meetings and conferences.

Local flip angle correction for improved volume T1-quantification in 3D dGEMRIC using the Look-Locker technique, Carl Siversson et al, Abstract and oral presentation at International Society for Magnetic Resonance in Medicine (ISMRM) meeting 2008, Toronto, Canada, no 5289

B1 inhomogeneity corrected T1-quantification for dGEMRIC using 3D Look-Locker technique with non-slice selective RF-pulses, Carl Siversson et al, Abstract and poster at the International Society for Magnetic Resonance in Medicine (ISMRM) meeting 2009, Honolulu, Hawaii, no 6717

Gradient echo assisted 3D Look-Locker - A method for improved volume T1-quantification accuracy applied to dGEMRIC, Carl Siversson et al, Abstract and poster at the International Society for Magnetic Resonance in Medicine (ISMRM) meeting 2009, Honolulu, Hawaii, no 6659

Repeatability of T1-quantification in dGEMRIC for three different acquisition techniques: 2D inversion recovery, 3D Look-Locker and 3D variable flip angle, Carl Siversson et al, Abstract and poster at the International Society for Magnetic Resonance in Medicine (ISMRM) meeting 2009, Honolulu, Hawaii, no 5258

Verification of the local flip angle correction method for T1 quantification using the Look-Locker technique, Carl Siversson et al, Abstract and poster at the European Society for Magnetic Resonance in Medicine and Biology (ESMRMB) meeting 2009: 26th Scientific Meeting, Antalya, Turkey, no 486

Phantom verification of B1 inhomogeneity correction for 3D variable flip angle T1 measurements, Carl Siversson et al, Abstract and e-poster at the International Society for Magnetic Resonance in Medicine (ISMRM) meeting 2011, Montreal, Canada, no 4487

The effects of B1 inhomogeneity correction for 3D variable flip angle T1 measurements in hip-dGEMRIC at 3T and 1.5T, Carl Siversson et al, Abstract and e-poster at the International Society for Magnetic Resonance in Medicine (ISMRM) meeting 2011, Montreal, Canada, no 3227

Table of contents

Introduction **11**

1.1 Objectives of this thesis 12

2. Diarthrodial joints **13**

2.1 Articular cartilage 14

2.2 The menisci 15

2.3 Osteoarthritis 16

2.4 Assessing cartilage quality 17

2.4.1 dGEMRIC 17

2.4.2 Other MRI based cartilage assessment methods 20

3. Magnetic resonance overview **22**

3.1 Nuclear spin 22

3.2 RF-pulses and echoes 24

3.2.1 B_1 inhomogeneity 25

3.3 Relaxation times 25

3.4 Gradients and image formation 27

Developing T_1 quantification techniques **29**

4.1 The inversion recovery sequence 29

4.1.1 2D-IR pulse sequence theory 30

4.2 The Look-Locker sequence 31

4.2.1 3D-LL pulse sequence theory 31

4.2.2 Implementing a 3D-LL sequence 32

4.2.3 The constant flip angle correction method 34

4.2.4 The local flip angle correction method 35

4.2.5 The precalculated flip angle correction method 37

4.2.6 Experimental flip angle correction methods 38
4.2.7 Optimizing the acquisition parameters 40
4.3 The variable flip angle method 41
4.3.1 3D-VFA pulse sequence theory 42
4.3.2 Optimizing the flip angles 43
4.3.3 Correcting for B_1 variations 43
4.3.4 Mapping the B_1 variations 45
5. In vivo studies 47
5.1 Repeatability of the T_1 quantification methods 47
5.1.1 Repeatability measurements 48
5.2 3D-LL dGEMRIC in the meniscus 49
5.2.1 Time-response study 50
6. Summarized conclusions 52
Future aspects 53
7.1 Improving the cartilage assessment 53
7.2 Automatic cartilage segmentation and 3D visualization 54
8. Afterword 55
9. Acknowledgements 56
10. References 58

Paper I 69
Paper II 79
Paper III 89
Paper IV 97

1. Introduction

In magnetic resonance imaging (MRI), strong magnetic fields are used to generate *in vivo* images reflecting specific chemical and physical properties of the tissue. Due to its diagnostic value, in combination with its non-invasive nature and the absence of ionizing radiation, MRI has become an important tool in modern health care.

In traditional MRI the resulting images always reflect a combination of several parameters. Although the weighting factors between these parameters can be widely adjusted, no single parameter can be extracted from just one image. For this reason the viewer is referred to solely qualitative evaluation of the images, in which subjective visual contrasts between objects are of primary interest.

Many methods have been proposed to allow the underlying physical parameters to be quantified. Most of these methods rely on two or more images, having very well-defined differences, from which the parameter in question can be extracted. Unfortunately, this approach makes many of these methods highly sensitive to undesired variations within the images.

There are several applications in which accurate quantification of the underlying physical parameters would be of benefit. A prominent such application is assessment of cartilage quality using the delayed gadolinium-enhanced MRI of cartilage (dGEMRIC) technique, in which accurate quantification of the T_1 parameter is of interest. To date, there are strong indications that the dGEMRIC technique is able to follow the development of cartilage diseases such as osteoarthritis, years before actual symptoms are shown. Since this disease is among the leading global causes for disabilities, with increasing incidence, it can be expected that methods for understanding the disease will be of high importance in the years to come.

MRI data is usually acquired in either two or three dimensions. A two-dimensional acquisition results in a single image, cut though the tissue in any direction, while a three-dimensional acquisition results in an entire volume of image data. The T_1 parameter required for dGEMRIC has traditionally been acquired in two dimensions due to the higher stability of such methods. Accurately acquiring the T_1 parameter in an entire three-dimensional volume within a reasonable timeframe is associated with a number of issues, primarily resulting from intrinsic inaccuracies within the MRI data. However, developing such three-dimensional methods is of high interest since it would allow for new and improved means of diagnostics, both in dGEMRIC and in other T_1 related techniques.

1.1 Objectives of this thesis

The aim of this work has been to develop and evaluate three-dimensional methods for fast and accurate quantification of the T_1 parameter. In order to achieve this, methods for correction of undesired B_1 variations within the images were also to be included.

The associated application was to allow the entire cartilage volume within a joint to be examined with dGEMRIC, instead of only a selected cross section as with previous methods.

Derived from the general aims, the following detailed objectives were formulated:

- To implement a workflow for accurate and reliable dGEMRIC using three-dimensional T_1 acquisition techniques.
- To develop and evaluate different three-dimensional T_1 acquisition techniques and also compare them to gold standard two-dimensional sequences, both in phantoms and *in vivo*.
- To develop and evaluate methods for correction of quantification errors for the different T_1 acquisition techniques.
- To utilize the developed T_1 acquisition techniques for studies of clinical interest, such as the repeatability between successive dGEMRIC measurements and the feasibility of performing dGEMRIC in the menisci.

2. Diarthrodial joints

Diarthrodial joints are the most flexible joints in the human body, found for instance in the knees and the hips. From an engineering point of view these joints are profound mechanisms designed with highly demanding technical specifications. Not only must they allow for smooth and stable operation, they must also be flexible in several degrees of freedom. Likewise must they also function for the duration of a lifetime, while being used millions of times per year handling forces many times that of the body weight.

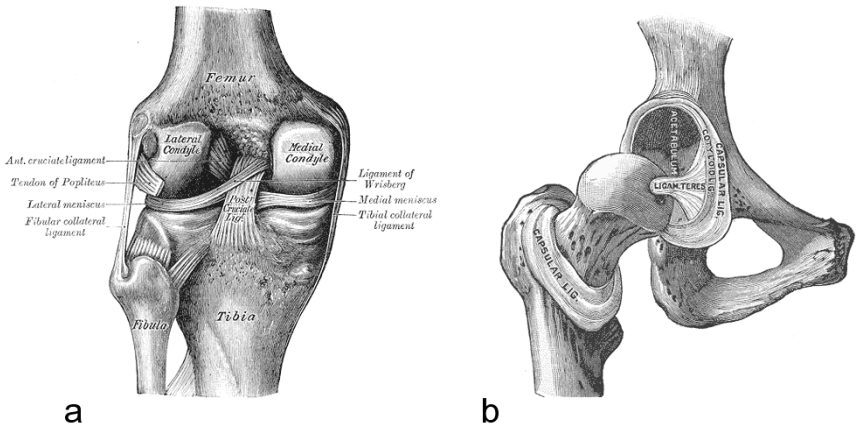

Figure 2.1 a) The knee joint as seen in the coronal plane **b)** The hip joint as seen in the coronal plane. The femur and the acetabulum are pulled apart for illustration (Gray, 1918).

All diarthrodial joints are enclosed in a strong fibrous capsule, in which the lubricating synovial fluid is secreted. Inside the capsule are the articulating bone ends, which are lined with a thin layer of hydrated soft tissue, i.e. the articular cartilage (Mow, 2005).

In the case of the knee joint (Fig. 2.1a) the articular surfaces are additionally supported by the meniscus. With its semilunar shape the meniscus extends around the articular surfaces, thereby off-loading the relatively limited contact area of the cartilage surfaces.

The hip joint (Fig. 2.1b) is instead a close-fitting ball-and-socket joint with shapes that are nearly spherical. As the socket (acetabulum) is normally a deep cup, this is a very stable joint with a large cartilage-to-cartilage contact area.

2.1 Articular cartilage

There are three major types of cartilage present in the body, all sharing the attribute of having chondrocytes as their only cell type. The primary distinction between the cartilage types lies within the biochemical composition and molecular structure of the extracellular matrices, which give rise to the distinct biochemical properties that are required for the function of each type of cartilage (Mow, 2005).

Articular cartilage belong to the hyaline type of cartilage, which in its healthy state is smooth, glistering and white in appearance. The primary role of the articular cartilage is to provide the joints with almost frictionless motion and to help absorb mechanical shock.

The articular cartilage should be regarded as a triphasic material (Lai, 1991). One major fluid phase consisting of interstitial water and another major solid phase primarily consisting of type II collagen and trapped proteoglycans. The third phase consist of dissolved electrolytes within the interstitial water.

The proteoglycans constitute 5-10% of the cartilage wet weight. The most occurring proteoglycan is aggrecan, which in turn are attached to hyaluronan acid, forming extremely large aggregated molecules. Each aggrecan molecule consist of a core protein with several covalently attached glycosaminoglycan (GAG) chains (Mow, 2005). These GAG chains are highly anionic and comprise up to 90% of the aggrecan molecular mass. The high negative charge has two effects. It repels the GAG chains from each other, thereby expanding their total volume (Mow, 1980). It also attracts counterions in the dissolved electrolytes which give rise to a Donnan osmotic pressure (Donnan 1924), increasing the water pressure within the extracellular matrix (Lai, 1991). Both these effects contribute to generate a swelling pressure within the cartilage.

In addition to this, there is the network of collagen fibers which provide both stiffness and tensile strength to the tissue (Mow, 1989), acting to restrain the swelling pressure generated by the GAGs. The combination of these effects makes the cartilage very durable with high compressive stiffness.

The composition of the cartilage tissue is not uniform throughout different depths. The cartilage is typically divided into three different zones. The superficial zone constitutes the outer 10-20% of the cartilage thickness and is characterized by the collagen fibers aligning parallel to the articular surface. It also has the lowest GAG level as compared with the other zones. The middle zone comprises 40-60% of the total thickness, having randomly aligned collagen fibers and the highest GAG level of the cartilage zones. In the remaining deep zone the collagen fibers form large bundles

that are organized perpendicular to the articular surface. At the bottom of the deep zone these bundles first cross the barrier into the calcified cartilage and are then inserted into the subchondral bone (Mow, 2001).

The water content of the cartilage decreases with depth, varying from about 80% in the superficial zone to about 65% in the deep zone. Much of this water comprises freely exchangeable interstitial water, which flows though the collagen-proteoglycan pores as the cartilage is compressed during motion. This flow induces additional forces within the tissue that are important to the physiology (Mow, 2005).

As a consequence of the depth-wise heterogeneity, the mechanical properties of the cartilage are changing at different depths. In combination with the varying thickness of the cartilage across the articular surface, this makes articular cartilage a highly sophisticated tissue designed for absorbing and distributing large forces without being damaged.

2.2 The menisci

The menisci primarily act to redistribute the contact force across the articulating surfaces within the knee joints. This is achieved though two opposing structures (lateral and medial) having wedge-like profiles, together forming a ring around the contact area of the two opposing cartilage surfaces (Fig. 2.2). It has been shown that even under heavy load the menisci are responsible for more than 60% of the total joint contact surface area (Walker, 1975).

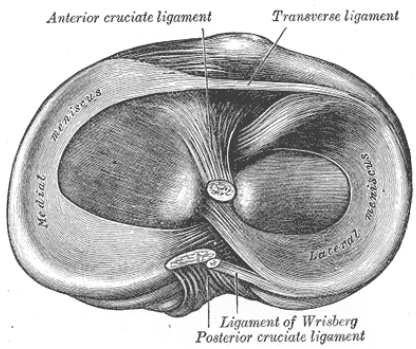

Figure 2.2 Head of right tibia as seen from above, showing the menisci and the attachments of ligaments (Gray, 1918).

The menisci belong to the fibrocartilage type, which is somewhat different from the hyaline articular cartilage. The peripheral parts of the menisci contain thick bundles of rope-like type I collagen fibers that are arranged along the direction of the structures (McDermott, 2010). Due to these fibers, the menisci can resist the expansion forces that occur when the joint is loaded. In contrast to the articular cartilage, the peripheral parts of the menisci also contain blood vessels, which allow the menisci to heal from certain types of damages (King 1936).

The inner regions of the menisci contain more randomly arranged smaller collagen fibers, resembling hyaline cartilage. These parts of the menisci do not contain any blood vessels and thus heal very poor from damages (Sommerlath, 1989).

In total, the menisci contain a slightly higher percentage of collagen than the articular cartilage. However, the percentage of proteoglycans in the menisci is much lower, only about 1-2% of the total wet weight (Mow, 2005), distributed denser in the inner region and more sparsely in the peripheral region (Verdonk 2010).

2.3 Osteoarthritis

Joint pain and loss of mobility due to degeneration of articular cartilage is among the most common reasons for disabilities in middle age and older people and is often associated with osteoarthritis (OA). For this reason OA has been ranked as one of the top ten diseases casing the highest global disease burden (WHO 2002).

OA is associated with a multitude of factors. Some of these are difficult to avoid, such as genetics and gender, while others are typically life-style related. OA commonly develops at older age, but it may as well develop earlier as a consequence of over-weight, trauma or otherwise disruption of cartilage integrity (Nuki 1999). OA can affect any diarthrodial joint but is often most cumbersome when affecting the weight bearing joints in the knees or hips.

During normal operation, cartilage matrix molecules are continuously degraded and replaced by newly synthesized molecules. This remodeling is controlled by the chondrocytes, which can synthesize and degrade all matrix constituents. Several studies have suggested that a metabolic imbalance occurs in OA (Koopman 1997).

The earliest histological effect in OA includes fibrillation of the cartilage in the superficial zone and decreased levels of proteoglycans. As more proteoglycans are depleted the fixed changed density within the cartilage will also decrease. This will result in a decreased swelling water pressure inside the cartilage, which with time will reduce the compressive stiffness and affect the mechanical properties of the cartilage (Mow, 2005). As the disease progress the cartilage will continue to break down until the subchondral bone is exposed at the articulating surface. At this stage, pain and immobility are often leaving no other choice than surgically replacing the joint with a prosthesis.

At earlier stages of the disease, the progress can sometimes be delayed by proper physical exercise in combination with pain-relieving treatments. A few surgical interventions exist, such as changing the alignment of the articulating bones ends with osteotomy (Parker, 2008). Also less invasive methods, such as using microfractures to generate cartilage-like repair tissue have been practiced in some types of OA (Braun, 2008; Yen, 2008).

2.4 Assessing cartilage quality

The traditional way of measuring the development of OA is based on radiographic images to determine the joint space width and the amount of OA related osteophytes (bone spurs) in the joint (Kellgren, 1957). Other relevant classification schemes also exist that are based on arthroscopic findings (Outerbridge 1961) or state of disease experienced by the patient (Roos, 1998; Bellamy 2002).

However, the degenerating biochemical processes associated with OA starts long before any of the above methods will any show signs of disease. In order for such early OA to be detected, novel MRI based methods have been developed that are directly sensitive to the chemical composition of the cartilage.

2.4.1 dGEMRIC

Delayed gadolinium-enhanced MRI of cartilage (dGEMRIC) is a technique for estimating the GAG content in the cartilage, thus providing information about the cartilage quality also at a very early stage of potential joint disease.

A negatively charged contrast agent (Gd-DTPA^{2-}) is administered intravenously. The contrast agent will then distribute from the blood via the synovium into the cartilage, where its uptake will be restricted by the repelling electrostatic forces from the negatively charged GAG. Thus, high uptake of contrast agent indicates low GAG content and vice versa (Bashir, 1996). Due to the paramagnetic nature of the gadolinium (Gd) compound, the concentration of contrast agent within the cartilage can be measured using an MRI scanner. More specifically, the parameter of interest is the longitudinal relaxation time (T_1) which relates to the contrast agent concentration by

$$[Gd] = \frac{1}{r_1} \cdot \left(\frac{1}{T_{1Gd}} - \frac{1}{T_{1pre}} \right) \qquad \text{Eq. 2.1}$$

where r_1 is the relaxivity of the contrast agent and $T_{1\mathrm{pre}}$ and $T_{1\mathrm{Gd}}$ are the measured T_1 values before and after contrast injection, respectively (Stanisz, 2000).

However, the $T_{1\text{pre}}$ value is relatively stable between patients and always much higher than the $T_{1\text{Gd}}$ value. For this reason the effect of the $T_{1\text{pre}}$ value for the [Gd] calculation is limited and is often omitted as that simplifies the logistic procedure significantly (Bashir, 1999; Li, 2009). For this reason many studies considers the $T_{1\text{Gd}}$ value as a stand-alone measurement of the GAG concentration, often denoted as "the dGEMRIC index" (Williams, 2007). Higher $T_{1\text{Gd}}$ value then indicates more GAG and vice versa.

Following the contrast administration, time must be allowed for contrast agent accumulation in the cartilage. Time-response studies have concluded that the MRI scan should be performed when the contrast concentration is at its maximum, which is at 90-120 minutes for the knee joint (Burstein, 2001; Tiderius, 2001) and at 30-60 minutes for the hip joint (Tiderius, 2007). After this the contrast level will start to decrease again due to the renal functions. During the delay between contrast administration and MRI scan a moderate exercise program is usually practiced in order to further enhance the contrast agent distribution (Burstein, 2001).

Within the resulting T_1 maps, that are generated by the MRI scanner, regions of interest (ROIs) are manually drawn from which average T_1 values are calculated. Such ROIs can be drawn in a variety of ways, mostly depending on which areas of the cartilage that are of interest for the particular study (Eckstein, 2006). Commonly, the ROIs are drawn within the weight-bearing part of the cartilage (Fig. 2.3) as early degenerative cartilage changes are most prone to occur there. It has been shown that such regions can be manually very well delineated. Thus, provided that the written guidelines are lucid, intra-observer variation should be very low when drawing these type of ROIs (Tiderius, 2004).

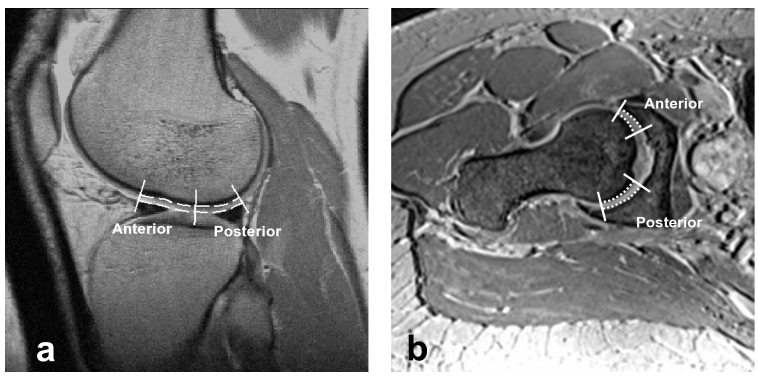

Figure 2.3 Typical set of ROIs in the **a)** knee and **b)** hip. ROIs constitute the thin section between the dashed lines, limited at the ends points by the solid lines.

Previous dGEMRIC findings

In the early days of dGEMRIC, studies were performed to establish the relationship between cartilage quality and $T_{1\mathrm{Gd}}$. From these studies it was concluded that $T_{1\mathrm{Gd}}$ is higher in physically active individuals than in sedentary individuals, which may indicate that the cartilage has an adaptive capacity (Tiderius, 2004). It was also concluded that in patients with early OA the $T_{1\mathrm{Gd}}$ value was even lower. In these patients no radiographic signs could be seen, only arthroscopic surface fibrillations (Tiderius, 2003).

Furthermore, studies have also been performed on meniscectomized patients, which are known to be at risk of developing OA, showing a low $T_{1\mathrm{Gd}}$ even before OA symptoms are shown (Ericsson, 2009). In another recent study a six year followup on previous dGEMRIC patients was performed, showing a significant relation between $T_{1\mathrm{Gd}}$ and the development of OA (Owman, 2008).

What is important to realize regarding these results is that they reflect the average for a specific category of subjects. When studying the results for an individual subject there can be large fluctuations compared to other individuals within the same category. This is especially the case for OA patients where inhomogeneities in the cartilage structure can be expected to a larger extent, as is reflected by the high standard deviation of the ”Early OA” group in Fig. 2.4.

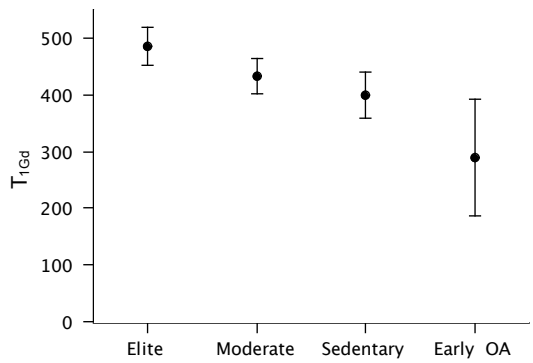

Figure 2.4 dGEMRIC $T_{1\mathrm{Gd}}$ values in articular knee cartilage for asymptomatic individuals at three different levels of physical exercise (Tiderius, 2004) together with $T_{1\mathrm{Gd}}$ values for patients with early OA (Tiderius, 2003). Measurements were performed with a triple-dose of contrast agent, using a 1.5T MRI scanner.

Issues related to dGEMRIC

Even though the basic theory behind the dGEMRIC technique is not very complicated, there are many issues that are yet to be understood. Among these are several factors, other than the GAG level, that may influence the measured $T_{1\mathrm{Gd}}$ value.

Recent studies suggest that due to concurrent wash-in and wash-out effects the distribution of contrast agent within the cartilage never reaches a true equilibrium and thus never levels out. Instead it seems that the maximum contrast concentration occurs momentarily and at different time points for different depths. Thus, the apparent optimal time window for the MRI scan (at 90-120 minutes for knees) might actually be an effect of the averaging that occurs from drawing the ROIs over the bulk depth of the cartilage (Lammentausta, 2011).

It is also shown that the GAG concentration varies at different depths, which makes it unclear to what proportion contrast distribution is affected by fixed charge density or other diffusion parameters (Li, 2010; Lammentausta, 2011).

It should be noted that some controversy exist regarding the contrast transport mechanism. The general opinion is that the contrast agent distributes into the cartilage via the synovial fluid only, as the diffusion through the underlying subchondral bone is very low. However, it has been suggested that there is a potential contrast distribution across the cartilage–bone interface in OA, due to angiogenic factors leading to growth of blood vessels (Murata, 2008; Li, 2010).

Concerns have also been raised regarding the relaxivity of the contrast agent not being as well determined as previously thought. It has been shown that the relaxivity varies with the amount of solid component of the tissue, which may mean that OA related changes other than the GAG level will also affect the measured T_1 value (Stanisz, 2000; Zheng, 2010).

A further concern is that the $T_{1\mathrm{pre}}$ value might vary more than previously anticipated at some stages of disease. These findings suggest that under certain conditions T_1 measurements should be preformed both before and after contrast agent injection (Tiderius, 2003; Watanabe, 2006).

In addition, there appears to be a relationship between body mass index (BMI) and contrast distribution, suggesting that obese and overweight people receive a lower dose of contrast agent per body weight, in order for their cartilage quality not to be underestimated (Tiderius, 2006).

2.4.2 Other MRI based cartilage assessment methods

Since the MRI scanner is able to generate a multitude of images in which various features are emphasized, a number of different MRI based cartilage assessment methods have been developed. Compared to dGEMRIC these methods have the advantage that they do not require a contrast agent, although they instead have other issues to consider. Regarding which method is the best, there is no definite answer.

Each method has both advantages and disadvantages, both in terms of diagnostic value and expensive equipment.

Cartilage T_2 measurements

Measuring T_2 involves quantifying the decay of transverse magnetization within the cartilage. The variation of T_2 has been studied in both knee and hip cartilage and the values seem to reflect a combination of several physical properties. Significant correlation has been reported between T_2 values and collagen structure (Nieminen, 2001) but it also seem to depend on proteoglycan levels (Regatte, 2002) and water content (Lusse, 2000). General sensitivities to degenerative changes (Menezes, 2004) as well as mechanical properties (Nieminen, 2004) have also been reported.

Cartilage $T_{1\rho}$ measurements

$T_{1\rho}$ [T_1 rho] measurements involve quantification of the longitudinal magnetization recovery at a magnetic field strength that is artificially reduced to a fraction of the actual field in the MRI scanner (Sepponen, 1985). Of most interest for OA research is commonly its reported relationship to proteoglycan content (Regatte, 2002; Wheaton, 2004). However, the $T_{1\rho}$ parameter is not exclusively sensitive to any specific component but rather to a combination of different effects.

gagCEST measurements

With gagCEST (GAG chemical exchange saturation transfer) the NH-groups within the GAG molecules are directly quantified, possibly resulting in a very accurate determination of the GAG level. To date very few publications are available in which this method is used, but the initial results seem promising (Ling, 2008; Schmitt, 2011). The relatively high demands on the MRI scanner might pose a limitation in some circumstances.

Sodium MRI

Sodium (Na) MRI directly measures the amount of Na-ions in the electrolyte surrounding the GAG molecules within the cartilage. As such, sodium MRI measures the actual fixed charge density (Reddy, 1997) and is often considered as the optimal method for GAG quantification. The downside is that due to the low concentration of Na-ions a very high field (7T) MRI scanner is recommended, which are not yet very widely adopted outside of a few dedicated research centers.

3. Magnetic resonance overview

In a typical MRI investigation a sample is placed in a strong static magnetic field, generated by a superconducting electromagnet, where the sample becomes temporarily magnetized. By exposing the sample to a series of radio frequency pulses and magnetic field gradients, the nuclei in the sample start to emit a radio frequency signal of its own. This signal is detected by the MRI scanner and formed into an image. In clinical MRI, the signal from the hydrogen nuclei are the most widely used, due to the abundance of hydrogen rich components such as water and fat in the human body.

In this chapter an overview of the MRI phenomena is given, based on information from a few of the excellent textbooks (Haacke 1999; Bernstein, 2004; Tofts 2004) available on this topic. What is presented here aims to communicate an intuitive understanding of the relevant concepts, rather than the full theoretical background about MRI. For such knowledge the reader is referred to any of the textbooks.

3.1 Nuclear spin

Protons and neutrons both have an intrinsic quantum property called spin. In an atomic nucleus the number of protons and neutrons determine whether the nucleus will have an overall spin or not. In the case of clinical MRI the hydrogen nucleus is of primary interest, which posses an overall spin since it consists of only a single proton.

In a strict sense, the spin of an individual nucleus should be described from a quantum physics perspective. That said, there are a number of spin models based on conventional physics that are not fully comprehensive, but which are still valuable as an intuitive basis for thoughts. In one such model the spin property can be described as each nucleus rotating around its own axis (Fig. 3.1). Since the nucleus is positively charged itself, the rotating charge is equivalent to a rotating current, generating a small magnetic field. Hence, each nucleus has its own intrinsic magnetic vector pointing along its axis of rotation.

Without external influences, the intrinsic magnetic vectors of nuclei in a normal tissue sample are pointing in totally random directions. Hence, from a macroscopic perspective these vectors are averaging themselves out to no net magnetization at all.

When placing nuclei in an external magnetic field, B_0, the intrinsic magnetic vector of each nucleus will align in the direction of the external field[1]. However, this alignment will not make these vectors become strictly parallel to the external field. Instead, the vectors will start to precess around the axis of the external B_0 field, with a rotational frequency called the Larmor frequency, v_0 (Fig. 3.1). This frequency varies with the strength of the external B_0 field by

$$v_0 = \frac{\gamma \cdot B_0}{2\pi} \qquad \text{Eq. 3.1}$$

where γ is a nuclei specific constant called the gyromagnetic ratio ($\gamma/2\pi$ = 42.6 MHz/T for the hydrogen nucleus).

In any tissue sample, even an extremely small volume contains many millions of hydrogen nuclei. For this reason it is instructive to consider a large number of nuclei as a single unit, called an isochromat (Fig. 3.2). The intrinsic magnetic vectors of each nucleus in an isochromat are all precessing about the B_0 field, but at random angular positions. Thus, adding all intrinsic vectors of the isochromat together, results in a bulk magnetization vector, M, pointing in the direction of the B_0 field.

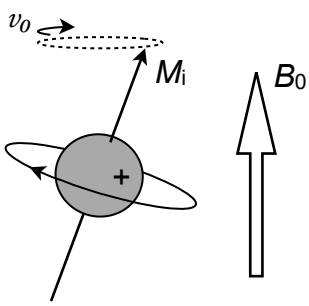

Figure 3.1. The hydrogen nucleus spins around its own axis, generating the magnetic vector M_i, which in turn makes the nucleus precess with the Larmor rotation frequency v_0 about the direction of the external field B_0.

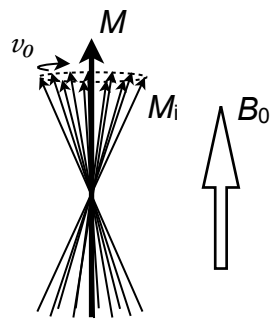

Figure 3.2 Each individual magnetic vector, M_i, has a random angular position. Thus, the sum of all M_i vectors in an isochromat is a new vector, M, pointing in the same direction as the externally applied B_0 field.

[1] Strictly speaking, there are are almost as many hydrogen nuclei aligned towards the B_0 field, with only a small surplus of nuclei aligned as described above.

3.2 RF-pulses and echoes

In order to interact with the precessing nuclei, radio frequency (RF) magnetic pulses are used. Such pulses are generated by an external coil in which the current is oscillating with the same frequency as the Larmor frequency. The oscillating magnetic field generated by such coil can be divided into separate components. Of particular interest is the component that is perpendicular to the B_0 field, which can be thought of as an additional magnetic field (called the B_1 field), rotating around the B_0 direction (Fig. 3.3).

For the nuclei there are now two concurrent magnetic fields around which they will precess. Since one of the fields is stationary (B_0) and the other is rotating (B_1), the result is that the bulk magnetization vector M will slowly spiral itself away from the B_0 direction. This spiraling will proceed for the duration of the RF pulse. Initially it will spiral downwards, until the magnetization vector M is completely inverted. If the RF pulse is applied past complete inversion, the vector M will spiral back up again.

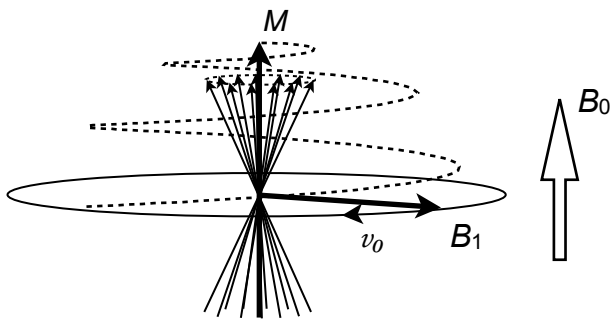

Figure 3.3 The RF pulse can be though of as a magnetic B_1 field rotating around the B_0 direction. The nuclei will then precess around both the B_0 and the B_1 fields, which results in the M vector spiraling away from the B_0 direction.

An RF-pulse is characterized by the resulting angle between the magnetization vector M and the B_0 direction. This flip angle is primarily determined by the duration and the amplitude of the generated B_1 field.

As soon as the M vector points away from the B_0 direction, it will no longer be time and space invariant. Thus, the magnetic field around the nuclei will be fluctuating, which can induce a signal in an external receiver coil. At 90° flip angle the M vector is perpendicular to the B_0 field and the generated signal will have its maximum amplitude.

The signal described here is called a FID (free induction decay), which is the most simple MRI signal to generate. However, in clinical MRI another type of signals are

more commonly used, which requires a few additional steps to generate. These signals are referred to as echoes and are characterized by being slightly delayed from the RF pulse, making them better suited for image formation. The two most common echo types are gradient echoes and spin echoes.

3.2.1 B_1 inhomogeneity

When an RF-pulse is applied the MRI scanner knows from calibration measurements which amplitude to use in order to achieve a specific flip angle, at least in average over the investigated object. However, different tissue types have different physical properties (such as density, conductivity and dielectric constant) causing small localized variations in the distributed B_1 field. In addition to this, the coil itself might not transmit a B_1 field that is entirely uniform in every position.

These types of variations can be regarded as inhomogeneities in the magnitude of the applied B_1 field, causing small variations in the flip angle at different positions in the investigated object. Such variations are always present and in some applications they may be very troublesome. However, there are ways to correct for these B_1 inhomogeneities, which is something that is thoroughly discussed throughout this work.

3.3 Relaxation times

When the magnetization vector M is perturbed by an RF pulse, it will take a certain amount of time until it is back in its equilibrium state (i.e. when the isochromats are fully relaxed). This time is determined by the longitudinal magnetization relaxation time and relates typically to the fluctuating magnetic field generated by other molecules in the neighborhood (dipole-dipole interaction).

The longitudinal (parallel to B_0) magnetization recovers exponentially with time and is characterized by the T_1 relaxation time, which is described by one of the Bloch differential equations

$$\frac{dM_z(t)}{dt} = \frac{M_0 - M_z(t)}{T_1} \qquad \text{Eq. 3.2}$$

where M_0 is the magnetization vector at equilibrium and $M_z(t)$ is the longitudinal component of the magnetization vector at a time t. More intuitively, the T_1 parameter can also be described as the time it takes for the nuclei to recover 63% of the longitudinal magnetization that was lost when the RF pulse was applied.

Another measure of relaxation is the time it takes for the emitted echo to decay (Fig. 3.4). This is determined by the transverse magnetization relaxation time[2] and is among other things an effect of how mobile the molecules are.

The transverse (perpendicular to B_0) magnetization decays exponentially with time and is characterized by the T_2 relaxation time, which is described by another of the Bloch differential equations[3]

$$\frac{dM_{xy}(t)}{dt} = -\frac{M_{xy}(t)}{T_2} \qquad \text{Eq. 3.3}$$

where M_{xy}(t) is the transverse component of the summarized magnetization vector from the dephasing nuclei at a time t (Fig. 3.4). More intuitively, the T_2 parameter can be described as the time it takes for the amplitude of an emitted echo to decline to 37% of what it was immediately after the RF pulse[2].

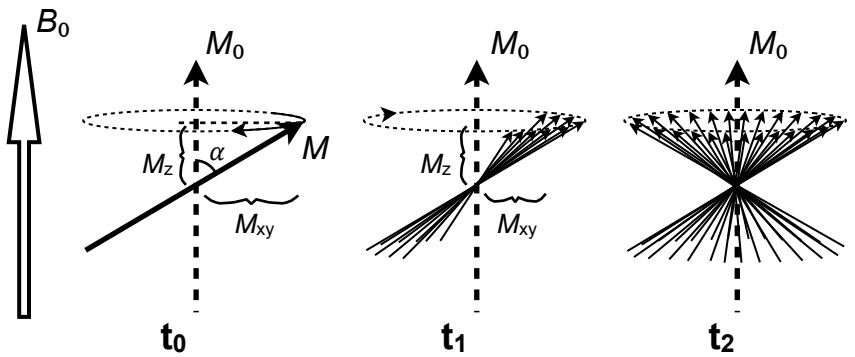

Figure 3.4 Immediately after an RF pulse (t_0) the magnetization vector M is perturbed from its initial M_0 direction by a flip angle α. M_z is the remaining longitudinal magnetization, which will eventually recover to back to M_0. At this point, the transverse magnetization component M_{xy} is time variant, allowing a signal to be induced in an external pick-up coil. A short while later (t_1) the individual spinning nuclei that make up the M vector have de-phased somewhat, resulting in a smaller time variant component M_{xy} and a decreased amplitude of the induced signal. After yet another while (t_2) the spinning nuclei have de-phased totally, resulting in no time variant component at all. At this point, no signal will be induced in the external coil. The de-phasing time is characterized by the T_2 parameter[2].

---

[2] This description is accurate if there are no local variations at all in the static magnetic field, which is never the case in reality. With variations the signal decays faster, which is characterized by the T_2^* parameter. This relation is described as $1/T_2^* = 1/T_2 + 1/T_2'$, where the T_2' parameter characterizes the local B_0 variations.

[3] This form of the equation assumes that the rotating frame of reference is used, i.e. that the observer rotates with the Larmor frequency the around the same axis as the magnetization.

3.4 Gradients and image formation

In order to form images it is necessary to be able to differentiate between signals coming from nuclei in different parts of the object. This is achieved using the gradient coils.

As the name implies, the gradient coils generate magnetic fields that are designed such that they vary linearly in strength along their axis of operation (Fig. 3.5). When the gradient is switched on, its field will superimpose itself onto the static magnetic field. The total magnetic field strength will then be somewhat higher in one end of the investigated volume and somewhat lower in the other end. Hence, the Larmor frequency of the nuclei in the volume will also vary throughout the different positions. This is the effect that is used to form images.

There are three sets of gradient coils in a clinical MRI scanner, generating magnetic field gradients in three orthogonal directions. By combining these three gradient coils (i.e. running them simultaneously) apparent magnetic field gradients can be generated in any direction. There are typically three different ways to use the gradients for encoding spatial information:

1. Applying a low-bandwidth RF pulse while a magnetic field gradient is switched on, will exclude all nuclei whose Larmor frequency is outside of the RF-pulse bandwidth.
2. Applying a gradient for a short while immediately after an RF pulse will create a difference in phase of pulses emitted from nuclei at different positions.
3. Applying a gradient during the echo will make nuclei at different positions emit signals with different frequencies.

Thus, by sampling each emitted echo and analyzing its phase and its frequency spectrum, information about nuclei from different parts of the subject can be obtained. However, all information required to generate an image can not be contained within one echo. Thus, the combination of gradients and RF pulses must be repeated many times, changing the gradient encoding slightly for each repetition, in order to obtain the information necessary to generate an image. Such combination of repeated gradients and RF pulses is denoted a *pulse sequence* and can be configured in a plurality of ways in order to enhance the obtained image for different purposes.

When a pulse sequence is executed, the sampled echoes together constitutes a frequency representation of the object, which can later be Fourier transformed into a real visible image. Such frequency representation is called a *k-space* image.

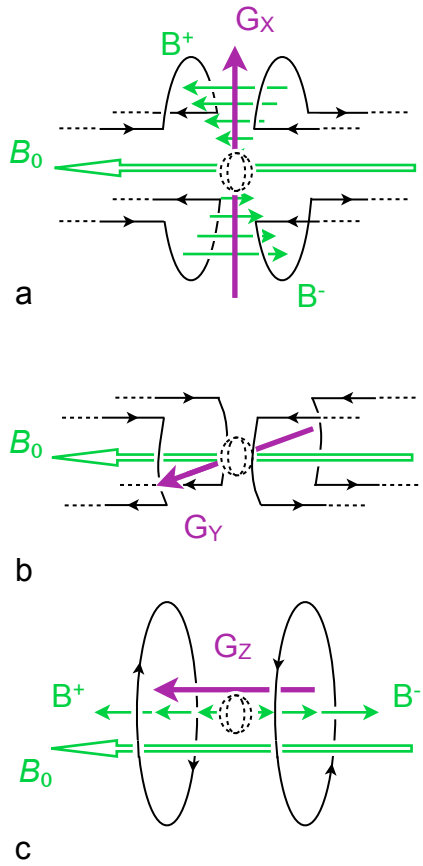

Figure 3.5 Three sets of gradient coils are built into the bore of an MRI scanner. The X and Y gradients (a and b) are similar, but aligned in different directions. Each gradient consist of two coils, generating two opposing magnetic fields (B^+ and B^-) which superimpose to a linear magnetic field gradient (G_X, G_y and G_z) through the central part of the bore, where the imaging is performed. Outside of the central part the gradient is not linear. The gradient field is in turn superimposed on the static B_0 field. By adjusting the current, the slope of the gradient is changed.

4. Developing T_1 quantification techniques

With conventional imaging methods the pixel intensity in an image represents a weighted combination of T_1, T_2 and proton density (PD). In order to exclusively retrieve a specific parameter most methods acquire two or more images, between which the differences are very well defined. The parameter in question can then be calculated.

The main focus behind this thesis is the development and evaluation of techniques for three-dimensional (3D) quantification of the T_1 parameter. The primary application is to allow dGEMRIC cartilage quality assessment that is not restricted to a single cross section, as the previous two-dimensional (2D) methods are. However, the techniques are useful for many other T_1 quantification applications as well.

In this chapter, the outcome of this work is presented, together with the supporting results of the dedicated phantom and *in vivo* studies that were performed.

Several MRI pulse sequences were used, some of which were programmed as part of this work, while others were provided as commercial products. The resulting MRI data was mostly evaluated using additionally created custom software, implementing both the relevant algorithms and providing a user interface for evaluations.

4.1 The inversion recovery sequence

Inversion recovery T_1 measurements are performed by perturbing the magnetization with an 180° inversion pulse and then observing the recovery of the longitudinal magnetization back to equilibrium (Gupta, 1980). This type of T_1 measurements are generally known to be both robust and accurate (Kingsley, 1998) and can be implemented using commonly available pulse sequences. The downside is that the measurements are relatively time consuming. Two-dimensional inversion recovery (2D-IR) was also the T_1 measurement method used in most of the early dGEMRIC studies (Bashir, 1999; Tiderius, 2001). For these reasons, 2D-IR has served as the gold standard for T_1 measurements in our work.

4.1.1 2D-IR pulse sequence theory

Following an inversion pulse, the nuclei are allowed to recover for a specific inversion time (TI), after which a 90° excitation pulse is applied (Fig. 4.1). The amplitude of the generated spin echo will then correspond to the amount of longitudinal magnetization at the specific TI. This is repeated a number of times, for different TI, thereby sampling the recovery of the magnetization at several different time-points.

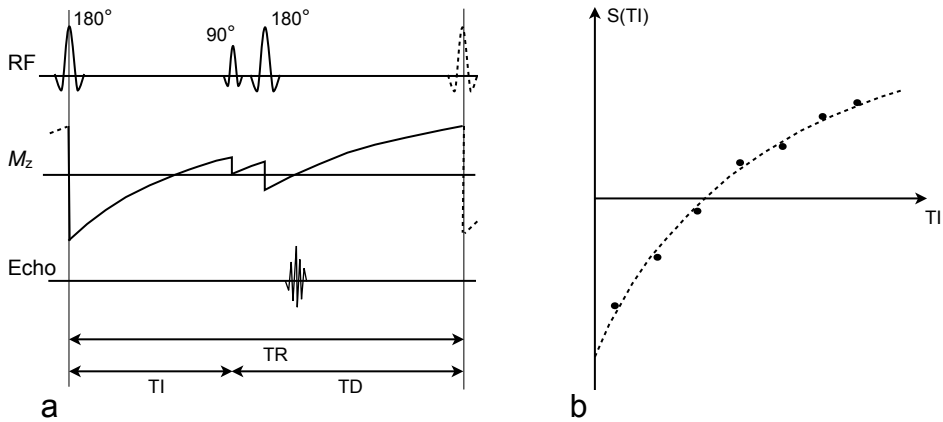

Figure 4.1 An inversion recovery sequence. **a**) A 180° inversion pulse is followed by a 90° excitation pulse which samples the longitudinal recovery (M_z) using a spin echo. The process is repeated for several different inversion times (TI). **b)** The amplitudes of the sampled echoes are fitted to a known longitudinal recovery curve (Eq. 4.1).

It has been shown that in the combined interest of time efficiency and T_1 measurement accuracy, the most optimal strategy is to keep the total repetition time (TR = TI+TD) constant (Kingsley, 1998). In such configuration, the T_1 value is retrieved by fitting the echo amplitudes to

$$S(TI) = S_0 \cdot (1 - 2 \cdot K \cdot e^{-TI/T_1} + e^{-TR/T_1}) \qquad \text{Eq. 4.1}$$

where *S(TI)* is the signal value at inversion time TI, retrieved using repetition time TR. *K* is the quality of the inversion pulse and S_0 is the signal that would be if the magnetization was allowed time to recover fully between the inversion pulses. The fitting procedure can take place using a three-parameter non-linear fitting algorithm of choice, for example the Levenberg–Marquardt algorithm (Levenberg 1944; Marquardt 1963).

In order to keep the acquisition time down, a series of spin echoes can be generated after each excitation pulse. Previous work have shown that such multiple spin echoes do not affect the T_1 quantification accuracy (Kingsley, 1998).

4.2 The Look-Locker sequence

Similar to the inversion recovery sequence, the Look-Locker sequence applies an inversion pulse after which the longitudinal magnetization is studied. However, instead of just a single excitation pulse, many consecutive excitation pulses are applied, continuously sampling the recovery. This allows for very fast T_1 quantification. The sequence was originally introduced by Look and Locker (Look, 1970) for use in nuclear magnetic resonance (NMR) spectroscopy. It was later modified for MRI in 2D (Hinson, 1988; Brix, 1990) which was followed by a 3D version (Henderson, 1999).

Two previous dGEMRIC studies have employed the 3D Look-Locker (3D-LL) sequence, showing encouraging results (Kimelman, 2006; Li, 2008). In this thesis much focus has been on improving the Look-Locker sequence to make its three dimensional T_1 quantifying capabilities more accurate. A series of phantom and *in vivo* studies was set up to verify the work (**Paper I**).

4.2.1 3D-LL pulse sequence theory

Following an initial 180° inversion pulse a continuous train of low flip angle excitation pulses are applied, from which gradient echoes are generated (Fig. 4.2). Since the pulses are of a low flip angle, only a small portion of the longitudinal magnetization is lost at each pulse, resulting in the longitudinal magnetization recovering until a steady state level is reached. This recovery can be quantified by fitting the amplitude of the echoes to the ordinary longitudinal magnetization recovery equation (Hinson, 1988), constituting a solution to one of the previously shown Bloch equations (Eq. 3.2).

However, due to the interference from the excitation pulses, the recovery retrieved from such fit will be faster than the true T_1 recovery. This apparent recovery is described by T_1*. The corrections required for recalculating this into the true T_1 value are discussed later in this chapter. The longitudinal magnetization recovery equation, with substituted variable names, is written as

$$S(TI) \propto M_Z(TI) = M_A - (M_A - M_B) \cdot e^{-TI/T_1^*} \qquad \text{Eq. 4.2}$$

where *S(TI)* is the amplitude of a Look-Locker echo at time TI following the inversion pulse. Variables M_A and M_B corresponds to values on the fitted curve at time-points zero and positive infinity, respectively (Fig. 4.2). The fitting procedure can be performed using a non-linear fitting algorithm of choice, for example the Levenberg–Marquardt algorithm (Levenberg 1944; Marquardt 1963).

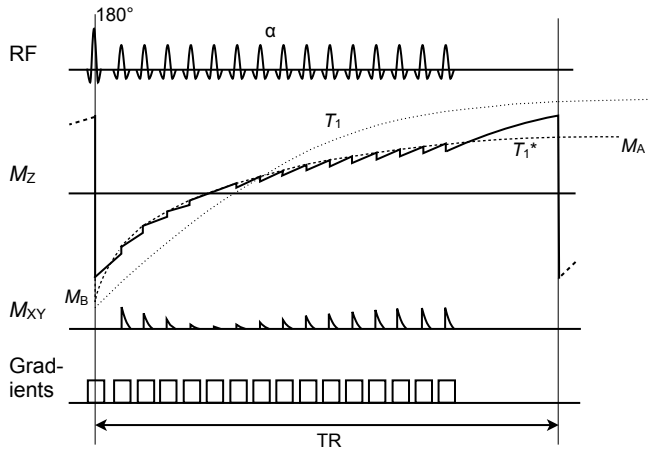

Figure 4.2 Schematic view of the Look-Locker sequence, showing the longitudinal magnetization evolution during a continuous train of excitation pulses with flip angle α. Due to the pulse train the magnetization recovers with an apparent T_1*, which is faster than the intrinsic T_1 recovery.

4.2.2 Implementing a 3D-LL sequence

Implementing a 3D-LL sequence involves encoding a large number of echoes into a plurality of k-spaces, in order to get a set of images representing the longitudinal magnetization at different time-points following the inversion pulse.

The configuration of pulses and gradients is essentially similar to that of a common spoiled multi gradient echo sequence, with the addition of a preceding inversion pulse. In the 3D-LL sequence that was designed as part of this work (Fig. 4.3, **Paper I**), an adiabatic inversion pulse is used for increased inversion accuracy while the excitation pulses are ordinary slice selective sinc pulses. Spoiling of transverse magnetization between the pulses is performed using a combination of RF-spoiling and a crusher gradient in the readout direction. The other gradients are balanced in order to avoid unpredictable spoiling behavior as the gradients are varying.

In a typical clinical application the longitudinal magnetization will reach a steady state level within a few hundred echoes. A proven way (Henderson, 1999) of organizing these echoes is to divide them into a number of groups corresponding to the number of desired points (TIs) along the recovery curve (Fig. 4.4). For each group there is an exclusive k-space, resulting in several different k-spaces receiving data for each train of excitation pulses following an inversion pulse. After a suitable repetition time the process is repeated, until each k-space has been filled with data.

After Fourier transform, each k-space generates a separate image volume, where each voxel has a signal amplitude corresponding to the magnetization in that voxel at the inversion time when the group was collected.

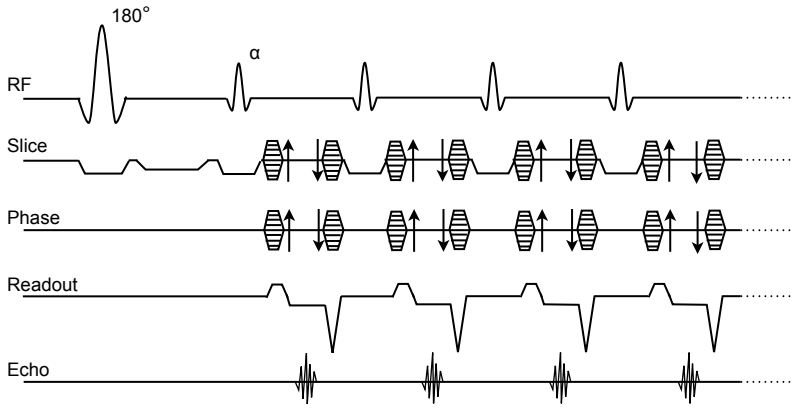

Figure 4.3 Our implementation of the 3D-LL pulse sequence. Variable α is the excitation pulse flip angle.

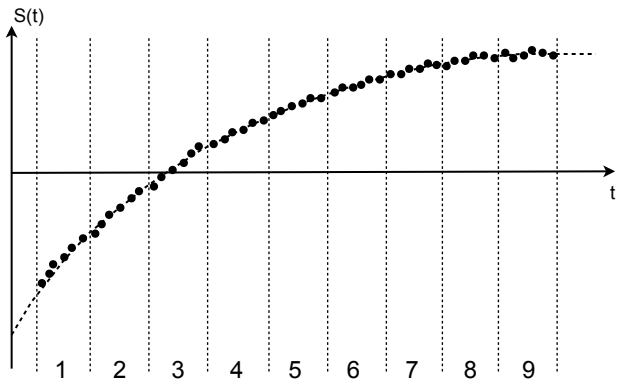

Figure 4.4 Successive echoes are divided into groups that are encoded into different k-spaces. Each k-space will generate an image volume corresponding to the inversion time at which the group was collected.

Effect of encoding schemes

In the 3D-LL sequence implemented in this work the echoes were organized such that each group contained all echoes required to fill an entire k_{xz} plane. While this was an easy approach for implementation, this method poses some restrictions on the resolution of the acquired data. For a large k_{xz} plane (i.e. high resolution in the slab direction, e.g. with isotropic acquisition) the magnetization evolution during the acquisition of such plane would be inappropriate (**Paper I; Paper II**). A simple way to solve this would be to split the acquisition of each k_{xz} plane into smaller parts.

Two different acquisition schemes were implemented for collecting the data within each k_{xz} plane. A linear scheme, where the lines were collected sequentially from one side to another, and a centric scheme, where the centermost line was collected first followed by the lines second closest to the center and so on. With centric encoding, the center of the first collected k-space will be earlier (i.e. closer to the inversion pulse), which should be beneficial for the curve fitting procedure. However, following evaluation of the two encoding methods it was concluded that there was no noticeable difference, neither in phantom measurements nor *in vivo* (**Paper I**).

4.2.3 The constant flip angle correction method

As previously mentioned the T_1* retrieved from fitting Eq. 4.2 to the Look-Locker data needs to be corrected in order to reflect the true T_1 value. As has been previously shown (Deichmann, 1991) this can be performed in a very simple way using

$$\frac{1}{T_1} = \frac{1}{T_1 *} + \frac{\ln(\cos(\alpha))}{t_f} \qquad \text{Eq. 4.3}$$

where α is the flip angles of the excitation pulse and t_f is the time between the excitation pulses. When this correction method is used, the nominal excitation pulse flip angle (as set in the user interface of the scanner) is used for all voxels. This is the method used in previously published dGEMRIC work involving the 3D-LL sequence (Kimelman, 2006; Li, 2008). In our work, this method is referred to as *the constant flip angle correction method* (**Paper I**).

However, one major drawback of this approach is that it requires the flip angle to be well determined in every voxel being corrected. In real measurements, this is unfortunately not usually the case, as the true flip angle will vary throughout different positions in the subject. One reason for this are B_1 inhomogeneities that are always present, especially *in vivo* (**Paper III**). Another reason is if a slab selective excitation pulse is used, which is usually the case for *in vivo* measurements in order to avoid fold-in artifacts from tissue outside of the field of view. Such pulse will always result in some flip angle variation throughout the direction of the slab selection gradient, since it is not possible to generate a finite length pulse that has a perfectly rectangular profile.

4.2.4 The local flip angle correction method

When the curve fit is performed, three parameters are retrieved that are all relevant in describing the evolution of the magnetization during the train of excitation pulses (see Eq. 4.2). The constant flip angle correction method, as described in section 4.2.3, only makes use of one of these parameters, which is also a reason for the problems associated with that method (Deichmann, 1991).

As a consequence of this we have developed a new method for calculating T_1, in which all three fitted parameters are used, together with all relevant timing information from within the sequence. With this method it is possible to correct the T_1* value in every voxel without *a priori* knowledge of the actual flip angle. We call this *the local flip angle correction method* (**Paper I**).

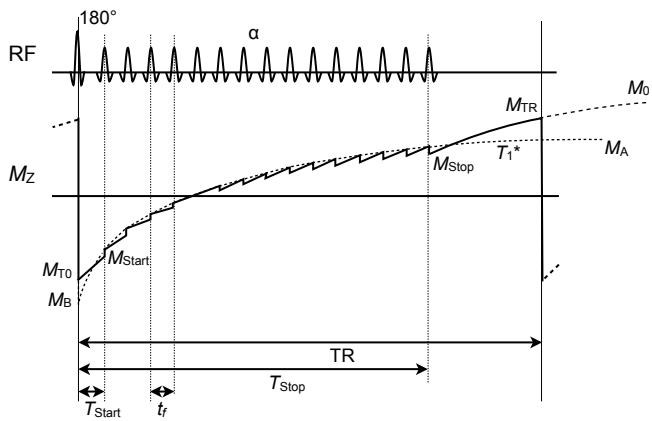

Figure 4.5 Look-Locker sequence diagram with all relevant timings and magnetizations annotated.

Referring to Fig. 4.5, M_A and M_B together with the parameter T_1* is retrieved from the previous three-parameter curve fit. A number of equations can then be set up describing the amount of longitudinal magnetization at different time-points. By combining those equations with Eq. 4.3 and the well known gradient echo steady state equation (van der Meulen, 1988) a new set of equations are retrieved which allow to solve T_1, without knowledge of the actual flip angle. This process is thoroughly described in **Paper I**. For clarity the resulting equations are summarized below.

$$M_{Tstart} = M_A - (M_A - M_B) \cdot e^{-\frac{T_{start}}{T_1^*}} \qquad \text{Eq. 4.4}$$

$$M_{Tstop} = M_A - (M_A - M_B) \cdot e^{-\frac{T_{stop}}{T_1^*}} \qquad \text{Eq. 4.5}$$

$$M_0 = \frac{M_{Start} + M_{Stop} \cdot K \cdot e^{-\frac{T_{start}}{T_1}} \cdot e^{-\frac{T_R - T_{stop}}{T_1}}}{1 - e^{-\frac{T_{start}}{T_1}} - K \cdot e^{-\frac{T_{start}}{T_1}} + K \cdot e^{-\frac{T_{start}}{T_1}} \cdot e^{-\frac{T_R - T_{stop}}{T_1}}} \qquad \text{Eq. 4.6}$$

$$T_1 = -\frac{t_f}{\ln\left(1 - \frac{M_A - M_A \cdot e^{-\frac{t_f}{T_1^*}}}{M_0}\right)} \qquad \text{Eq. 4.7}$$

Eqs. 4.4 and 4.5 only serve to calculate two values, which are directly inserted into Eq. 4.6. Hence, in Eqs. 4.6 and 4.7 there are three unknown variables left; T_1, M_0 and K. While the first two are self explanatory, the K value is a measure of the quality of the inversion pulse ($0<K<1$). Thus, if the inversion pulse quality is known or can be estimated, both T_1 and M_0 can be extracted separately from these equations.

As mentioned, the inversion pulse quality K, is still unresolved from the above equations. Depending on the type of inversion pulse used and the physical properties of the investigated sample, it may or may not be possible to perform a proper estimation of this parameter.

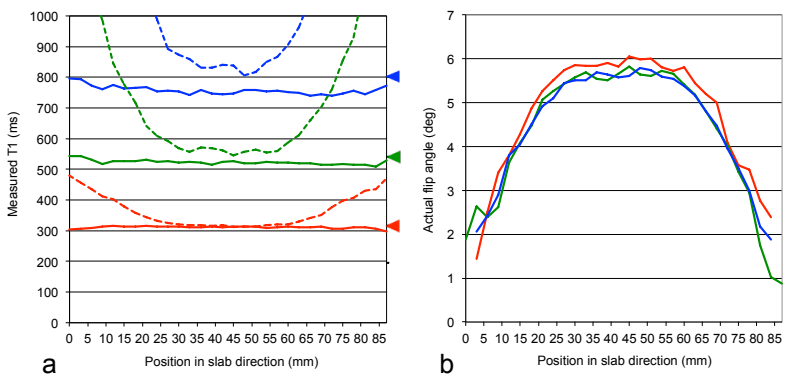

Figure 4.6. 3D-LL measurements throughout the slab selection direction of three phantoms. **a)** Solid lines are T_1 values with local flip angle correction. Dashed lines are T_1 values with constant flip angle correction. Arrows to the right are T_1 values for each phantom measured with 2D-IR. **b)** Calculated average flip angle profile through each phantom (using Eq. 4.8). The nominal flip angle was 6°.

In our 3D-LL sequence an adiabatic inversion pulse was implemented, in the belief that this would avoid uncertainties regarding the quality of the inversion. For phantom measurements this assumption was shown to be true, as the local flip angle correction method calculated excellent T_1 values throughout all parts of the volume (Fig. 4.6) (**Paper I**).

However, for *in vivo* measurements the method does not seem to perform with a similar perfection, as the calculated T_1 values are systematically underestimated. Our conclusion is that this likely is an effect of the inversion pulse not performing as good *in vivo* as it does in phantoms, in spite of it being adiabatic (Fig. 4.7) (**Paper I**).

4.2.5 The precalculated flip angle correction method

In situations when the inversion quality cannot be properly estimated, it will be necessary to calculate the true excitation pulse flip angle in each voxel by other means. The acquired T_1^* for a voxel can then be corrected using the calculated flip angle in combination with Eq. 4.3.

If it can be assumed that the main source for flip angle variations within a sample is due to the shape of the RF-pulse excitation profile, the actual flip angle will mostly depend on the position in the slab direction. Thus, by first mapping the flip angle slab profile, the acquired T_1^* from any voxel can be effectively corrected using the position in the slab direction in combination with the known slab profile. We refer to this method as *the precalculated flip angle correction method* (**Paper I**).

It should be noted that this type of correction does not correct for any actual B_1 inhomogeneities, as those are dependent on the composition of the actual object being scanned. Only the effects of the RF pulse slab profile not being perfectly rectangular are accounted for.

The slab profile can be estimated either by analyzing the RF-pulse waveform analytically or by measuring the shape of the pulse using an appropriate pulse sequence. In this work the second alternative was chosen, as that would make it easier to export the technique to other sites (**Paper I**). The profile is created by first running the 3D-LL sequence in an environment where the inversion quality is well defined, such as with a set of phantoms. The flip angle in each position in the slab direction is calculated by rewriting Eq. 4.3 as

$$\alpha = \arccos\left(e^{t_f\left(\frac{1}{T_1}-\frac{1}{T_1^*}\right)} \right) \qquad \text{Eq. 4.8}$$

and inserting the T_1 value acquired using the local flip angle correction method in combination with the corresponding T_1^*.

This retrieved slab profile will then be valid for correction of any other Look-Locker data acquired using the exact same excitation pulse, regardless of the quality of the inversion.

When comparing *in vivo* results of this method to *in vivo* results of the two other 3D-LL correction methods, the results of this method are superior (Fig. 4.7) (**Paper I**).

As a side note, it should be kept in mind that these data were acquired at 1.5T. At higher field strength (3T and above) the B_1 inhomogeneities are more significant (**Paper III**). In such situation the performance of the precalculated flip angle correction method should decrease.

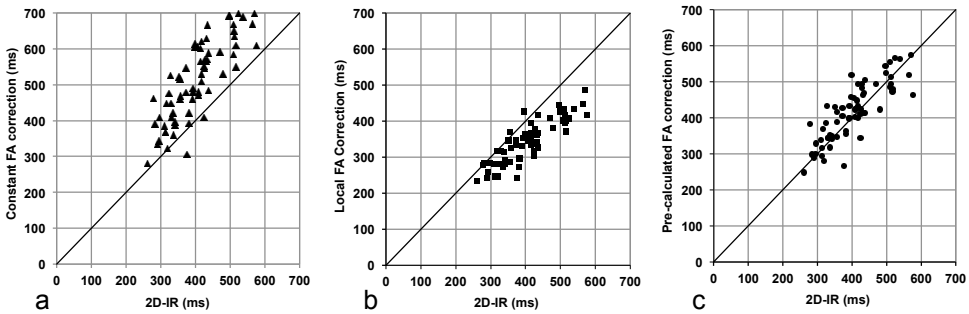

Figure 4.7 Data from a 1.5T dGEMRIC study (**Paper I**) with 66 *in vivo* measurements in weight-bearing knee cartilage using both 3D-LL and 2D-IR. The 3D-LL data is evaluated using each of the three evaluation methods and compared with T_1 measured using 2D-IR. The diagonal is a reference line. **a)** Constant flip angle correction versus 2D-IR **b)** Local flip angle correction versus 2D-IR **c)** Precalculated flip angle correction versus 2D-IR

4.2.6 Experimental flip angle correction methods

In addition to the described correction methods, we have also developed two experimental methods that have been briefly investigated. Both of these methods are extensions of the local flip angle correction method, involving additional correction for the inversion pulse quality. If successful, these methods are able to perform full correction for all unknown parameters that may affect the T_1 calculation.

Non-slab selective flip angle correction

In the first of these methods, both the adiabatic inversion pulse and the selective excitation pulses in the original sequence are exchanged for non-selective rectangular pulses. Thus, the same pulse shape is used for both excitation and inversion.

Due to this change in design it can be assumed that the inversion pulse is precisely as affected by any B_1 inhomogeneities as the excitation pulse is, resulting in a relationship

$$K = -\cos\left(\frac{\alpha}{\alpha_{Nom}} \cdot \pi\right) \qquad \text{Eq. 4.9}$$

where α and α_{Nom} are the actual and the nominal flip angles, respectively, for each voxel (Siversson, 2009). By combining this equation with the previously presented Eqs. 4.4 to 4.7, it is possible to solve both T_1 and M_0 without any unknown variables.

A small preliminary *in vivo* study was performed with this method (Siversson, 2009), showing very promising results (Fig. 4.8) as compared to the results of the other correction methods (Fig. 4.7).

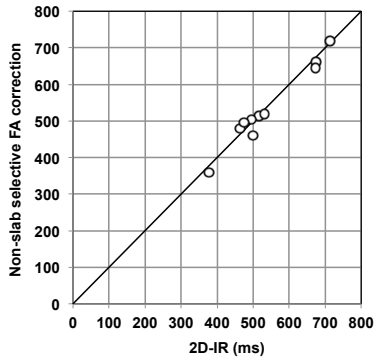

Figure 4.8 Data from a preliminary dGEMRIC study with 10 *in vivo* measurements in weight-bearing knee cartilage, comparing non-slab selective 3D-LL to 2D-IR (Siversson, 2009). The diagonal is a reference line. Measurements were performed at 1.5T.

The most obvious disadvantage of using non-selective pulses is that there will be folding artifacts if the investigated subject extends outside of the slab coverage. When examining such body parts as the hips, it is usually hard to avoid these effects, whereas with thinner extremities this is usually not a problem at all. Hence, this method seem very well suited for knee studies.

Gradient echo assisted flip angle correction

With this method an additional gradient echo sequence is executed right after the ordinary 3D-LL sequence, using a flip angle different from that of the 3D-LL sequence (Siversson, 2009). The basic idea is that since the excitation pulses of both sequences will be affected equally by B_1 variations, there will be only one specific inversion quality, K, for which the M_0 level of both sequences will be the same. Hence, equations can be set up solving all unknown variables, including the previously unknown K value .

A series of initial phantom test showed very promising results with this method (Siversson, 2009), but later *in vivo* results were very noisy. It is unclear if this was due to a non-optimal set of parameters or if it is an intrinsic design flaw of the method. For this reason no more work was put into the development, although it is not excluded that this may have potential to be a successful T_1 measurement method.

4.2.7 Optimizing the acquisition parameters

Very little information has been previously published regarding how to optimize the acquisition parameters for the Look-Locker sequence. For this reason a brute-force approach is taken in this work, finding the optimal set of parameters numerically using computer simulations.

A few of the 3D-LL parameters follow directly from the acquisition requirements and can thereby be regarded as static during the optimization process. This includes the time between the excitations pulses (t_f in Fig. 4.5), which should be minimized in order for as much information as possible to be acquired during each repetition. It also includes the time between the inversion pulse and the first excitation pulse (T_{start} in Fig. 4.5) which should be minimized in order for the first TI time to be as short as possible.

The exact length of the train of excitation pulses is not critical, but it should be long enough for the magnetization to approach a steady-state level, also for the highest T_1 values that are of interest. In the particular sequence implementation used in this work, the time between the TIs is determined by the number of phase encoding steps in the slab direction (see section 4.2.2) (**Paper I**).

The primary parameters that remain to be optimized are the nominal value of the excitation pulse flip angle and the delay time between the last excitation pulse and the inversion pulse (TR-T_{stop} in Fig. 4.5). This can be performed using a computer simulation of the 3D-LL sequence, where the sought parameters are sequentially adjusted in order to minimize the difference between the calculated T_1 value and true T_1 value. However, what is most likely to make a T_1 calculation of this type misbehave is the presence of noise. For this reason a reasonable amount of noise must also be added to the simulated echoes. The simulation must then be repeated a large number of times, in order to calculate both the average and the standard deviation of the retrieved T_1 values, for each set of tested parameters.

A series of such computer simulations were made for a variation of noise levels and T_1 values, using the same set of static parameters as in the real *in vivo* studies. From these simulations it was seen that as the noise level is increased, fewer combinations of delay times and flip angles generate accurate T_1 values. It was also seen that as the T_1 value is varied the optimal flip angle is slightly changed.

In order to find an appropriate set of parameters for *in vivo* usage a simulation was performed in which the T_1 value and the noise levels are similar to what can be expected *in vivo* (Fig. 4.9). In order to keep the total acquisition time down, the delay time should be chosen as low as possible. Also, in order to allow for some flip angle loss due to the slab profile, the flip angle should be as high as possible. From the diagram it can thereby be concluded that a nominal flip angle of 6-7° and a delay time of 700-800 ms are appropriate *in vivo* parameters. Such delay time yields a repetition time (TR) of about 2400 ms with the static parameters used in this simulation.

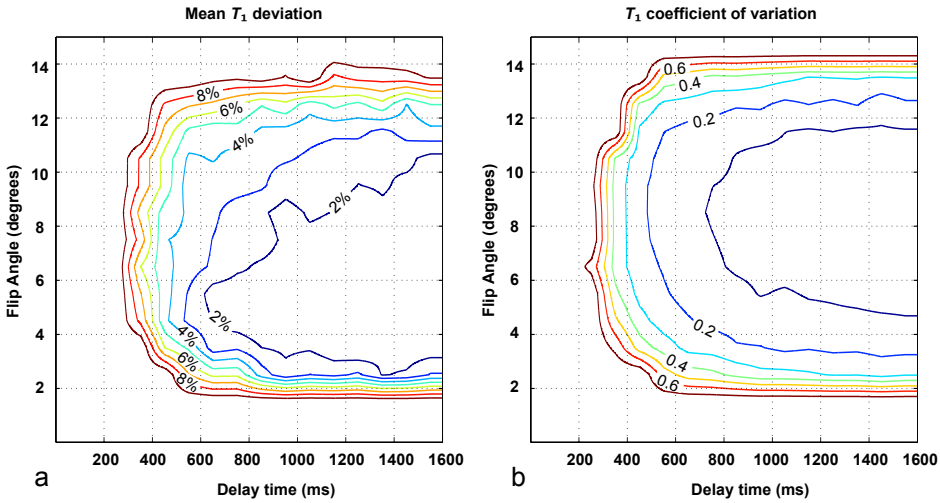

Figure 4.9 Computer simulation of the 3D-LL sequence for different flip angles and delay times (TR-T_{stop}). Evaluation is performed using the local flip angle correction method. Static parameters are t_f=5 ms, T_{Start} = 10 ms, 10 TIs, 31 excitations per TI. Simulated T_1 is 400 ms and the noise level is similar to what is present in an *in vivo* knee measurement. **a)** Deviation of calculated mean T_1 from true T_1. **b)** Coefficient of variation of calculated T_1.

4.3 The variable flip angle method

The variable flip angle method takes a different approach to T_1 quantification, as compared to the inversion pulse based sequences previously described. With this method T_1 is calculated using two or more successive spoiled gradient echo imaging sequences applied with different excitation pulse flip angles (Homer, 1985). Consequently, very rapid 3D variable flip angle (3D-VFA) T_1 quantification can be implemented using standard 3D gradient echo sequences (Brookes, 1999).

Several dGEMRIC studies have been published using 3D-VFA T_1 measurements, mostly showing promising results (Trattnig, 2007; Mamisch, 2008; Andreisek, 2009). In our work, studies have been performed to evaluate the impact of the magnetic field strength and its associated B_1 field inhomogeneities, on the accuracy of the T_1 measurements (**Paper III; Paper II**).

4.3.1 3D-VFA pulse sequence theory

A spoiled gradient echo sequence primarily consist of a train of low flip angle excitation pulses (Fig. 4.10). From each pulse a gradient echo is generated, which is encoded to a specific line in k-space. Remaining transverse magnetization after the echo is removed using RF or gradient spoiling (van der Meulen, 1988).

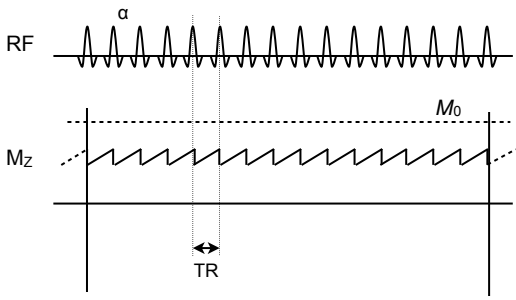

Figure 4.10 The longitudinal magnetization reaches a steady-state level in a standard spoiled gradient echo sequence.

After a number of such RF-pulses, the longitudinal magnetization will reach a level where exactly as much magnetization is recovered between pulses as is lost at each pulse. This is denoted the longitudinal steady state level, at which a signal S is generated, determined by

$$S = M_0 \cdot \frac{1 - e^{-\frac{TR}{T_1}}}{1 - e^{-\frac{TR}{T_1}} \cdot \cos(\alpha)} \cdot \sin(\alpha) \qquad \text{Eq. 4.10}$$

where α is the flip angle of the excitation pulses and TR is the time between the pulses (van der Meulen, 1988).

As can be seen, the steady state level is also dependent on the T_1 value. By running the same gradient echo sequence twice, with all parameters equal except the flip angle, two separate instances of Eq. 4.10 can be set up. Since M_0 will be equal in both these instances, is has been shown that the T_1 value can be solved by

$$T_1 = \frac{TR}{\ln\left(\frac{S_2 \cdot \sin(\alpha_1) \cdot \cos(\alpha_2) - S_1 \cdot \sin(\alpha_2) \cdot \cos(\alpha_1)}{S_2 \cdot \sin(\alpha_1) - S_1 \cdot \sin(\alpha_2)}\right)} \qquad \text{Eq. 4.11}$$

where S_1, α_1, S_2 and α_2 are the steady state levels and the flip angles of the first and second gradient echo sequences, respectively (Homer, 1985).

4.3.2 Optimizing the flip angles

For the 3D-VFA method to perform optimally, the flip angles must be selected with regard to the T_1 value to measure. In situations when accurate T_1 measurements are required over a wide range of T_1 values, acquiring data for more than two flip angles may be required (Deoni, 2004).

For any T_1 value and repetition time there will be a specific flip angle at which the signal from the gradient echo sequence has a maximum (Eq. 4.10), denoted the Ernst angle (Ernst, 1966). It has been shown that the optimal flip angle combination for a 3D-VFA T_1 measurement are the two flip angles for which the signal is 71% of that at the Ernst angle (Fig. 4.11) (Deoni, 2003). With this flip angle combination the calculated T_1 values will be least sensitive to any acquired noise.

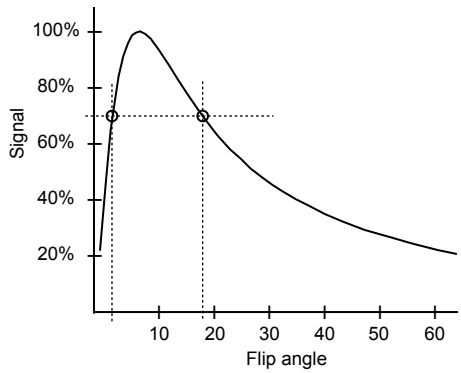

Figure 4.11 Steady-state gradient echo amplitude as a function of the excitation pulse flip angle (Eq. 4.10), for some arbitrary T_1 and TR. The optimal 3D-VFA flip angle combination is marked with circles.

4.3.3 Correcting for B_1 variations

The 3D-VFA sequence requires knowledge about the flip angles of the comprised gradient echo sequences in order for the T_1 value to be calculated (Eq. 4.11). The most widely used way of achieving this in dGEMRIC is to simply assume that the nominal flip angles, as specified in the user interface of the scanner, are sufficiently accurate and use them for T_1 calculation in the entire volume (Trattnig, 2007; Mamisch, 2008). While this may generate accurate T_1 values under some circumstances, there are a number of effects that may be hard to predict which can cause the actual flip angle to deviate severely, resulting in erroneous T_1 calculations (**Paper II**). Especially at high magnetic field strength (i.e. 3T), these effects may cause unacceptable errors (Fig. 4.12) in dGEMRIC measurements (**Paper III**).

This can be corrected for if a B_1 map can be calculated, measuring the relative difference c, between the nominal flip angles and the actual flip angle for each measured voxel, as described by

$$\alpha_1 = c \cdot \alpha_{1,Nominal} \qquad \text{Eq. 4.12}$$

$$\alpha_2 = c \cdot \alpha_{2,Nominal} \qquad \text{Eq. 4.13}$$

Such B_1 map can be calculated using an additional measurement sequence. The corrected α_1 and α_2 angles for each voxel are then used for input in the ordinary T_1 calculation (Eq. 4.11) resulting in a B_1 inhomogeneity corrected T_1 map (Gowland, 2004).

Since variations in the B_1 field are usually expected to be slowly varying, the B_1 map can be acquired with a very low resolution (Stollberger, 1996). In a typical clinical setup the resolution of the B_1 map is usually several times lower than that of the T_1 map. For this reason a complete B_1 map can be acquired in a very short time.

The 3D-VFA sequence with this type of B_1 correction have been tested in a few recent dGEMRIC publications, noticeably improving the T_1 quantification, both at 1.5T (Andreisek, 2009; Manuel, 2011) and at 3T (Fig. 4.12, **Paper III**).

It should be noted that when using a separate B_1 mapping sequence, flip angle variations resulting from the slab profile of the excitation pulse of the 3D-VFA sequence will not be corrected for. For this reason the outer parts of the T_1 volume, in the slab direction, will return erroneous T_1 values. A possible way around this could be to use a precalculated slab profile in combination with the B_1 mapping sequence (see section 7.1). However, in this work this was not an issue, since the T_1 measurements were restricted to the central part of the acquired volume.

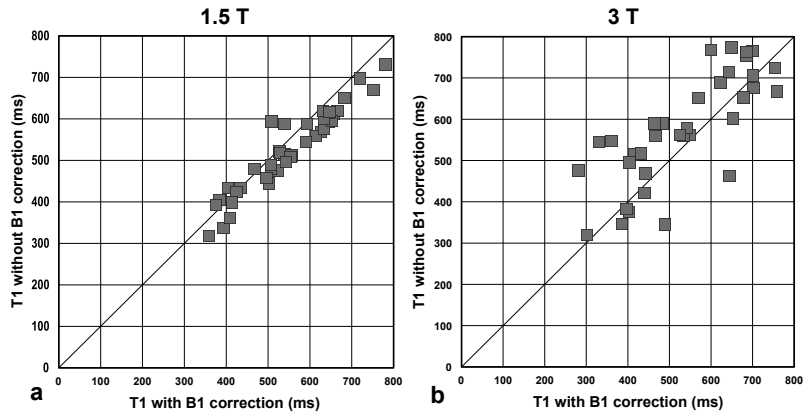

Figure 4.12 Data from an *in vivo* 3D-VFA dGEMRIC study (**Paper III**) in weight-bearing hip cartilage, with and without B_1 correction. The diagonal is a reference line. **a)** 40 measurements at 1.5T **b)** 40 measurements at 3T

4.3.4 Mapping the B_1 variations

There is a variety of sequences available for mapping the transmitted B_1 field strength. The two main types are the ratio based and the phase based methods, measuring the B_1 field strength from either the ratio of two echoes (Hornak, 1988; Carlson, 1990; Yarnykh 2007) or as a phase difference between two echoes (Oh, 1990).

In this work, a 2D multislice sequence, consisting of three consecutive pulses with the same flip angle, was used to map the transmitted B_1 field strength using a ratio based method (Perman, 1989). With this sequence the first pulse is an excitation pulse, which is followed by a second refocusing pulse, generating a spin-echo, and a final refocusing pulse generating a stimulated echo. From this the flip angle of the pulses, β, can be calculated using

$$\cos(\beta) = \frac{S_{STE} \cdot e^{t_p/T_1}}{S_{SE}} - 1 \qquad \text{Eq. 4.14}$$

where t_p is the time between the two refocusing pulses and S_{SE} and S_{STE} are the signal amplitudes from the spin echo and the stimulated echo, respectively. The requested B_1 correction factor (see Eqs 4.11 and 4.12) is calculated using

$$c = \frac{\beta}{\beta_{Nominal}} \qquad \text{Eq. 4.15}$$

where $\beta_{Nominal}$ is the nominal flip angle for the B_1 mapping sequence. In this work a nominal flip angle of 90° was chosen, in order to maximize the amplitudes of both the spin echo and the stimulated echo (Perman, 1989).

Even though the spin echo and the stimulated echo are only separated by typically 10-20 ms, the amount of T_1 relaxation taking place during this period must be accounted for. This is the reason for the exponential factor in Eq. 4.14, which requires that the T_1 value of the tissue is known. However, from phantom measurements it was concluded that using a constant T_1 value in the same regime as the true T_1 value, yields sufficient accuracy for dGEMRIC B_1 mapping (Fig. 4.13, **Paper III**). Depending on the technical setup, this assumption may simplify the measurements, as it makes the B_1 mapping sequence independent of input from other sequences.

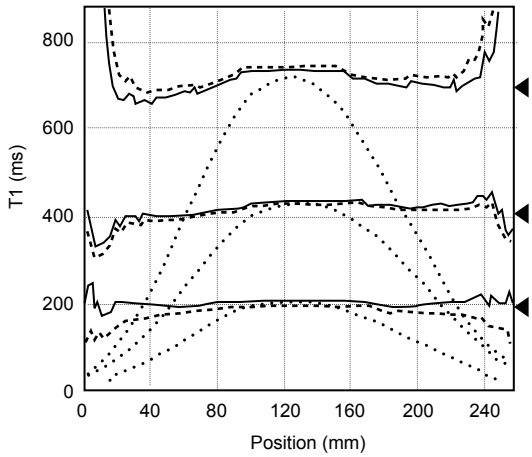

Figure 4.13. Measured T_1 along the centerlines of three long phantoms. The phantoms are placed in a transmitting extremity coil, extending out of the coil into the regions where the transmitted B_1 field is very low. Dotted lines are T_1 values calculated without taking the B_1 variations into account. Solid lines are B_1 corrected T_1 values, where the B_1 values are calculated using the true T_1 values for each of the phantoms. Dashed lines are B_1 corrected T_1 values, where the B_1 values are calculated for a constant T_1 of 500 ms. Reference T_1 values measured using 2D-IR are shown with arrows to the right (**Paper III**).

5. In vivo studies

As is mentioned in the previous chapter, several *in vivo* studies have been performed during the course of this work, mainly as part of the development of new measurement methods. In addition to this, two studies have been performed in which the clinical findings were in focus.

The purpose of these studies have been the combined interest of gaining deeper knowledge about OA while also verifying the new measurement methods in a clinical setup.

5.1 Repeatability of the T_1 quantification methods

The repeatability of the dGEMRIC method is an important issue, not only to evaluate the measurement techniques themselves, but also to gain further knowledge of the processes behind the dGEMRIC method. Since there are many factors, other than the GAG concentration, that might affect the measured T_1 in dGEMRIC, it is important to determine how persistent the measured T_1 results are between successive examinations.

Prior to this work, only one full study (Multanen, 2009) and one preliminary investigation (Burstein, 2001) had been performed regarding repeatability in knee-joint dGEMRIC measurements. Both of these were using the 2D-IR technique to investigate a group of healthy subjects. Whether or not the reported repeatability results would also pertain for patients with expected OA, where other factors may affect the outcome, was yet to be investigated.

For this purpose a study was performed with nine subjects, examined twice with a two-week interval, using the same dGEMRIC protocol at both occasions (**Paper II**). All subjects were recruited from a cohort previously sustaining a total anterior cruciate ligament (ACL) injury which put them at high risk of developing OA (Lohmander, 2007; Neuman, 2008).

For each examination, measurements were performed using each of the three different T_1 measurement methods (2D-IR, 3D-LL and 3D-VFA). The 3D-LL data was evaluated using the precalculated flip angle correction method, since previous studies concluded that those results are the most accurate (**Paper I**). It may be noted that the 3D-VFA measurements were performed without B_1 correction, which was common practice at the time of the study (**Paper III**).

5.1.1 Repeatability measurements

For each acquired T_1 map, ROIs were manually outlined in the anterior and posterior weight bearing cartilage regions of each condyle (as in Fig. 2.3a) and the mean T_1 value for each ROI was calculated. The difference in T_1 value between the first and second measurements for each ROI was then evaluated statistically in order to derive a measure of repeatability for each measurement method.

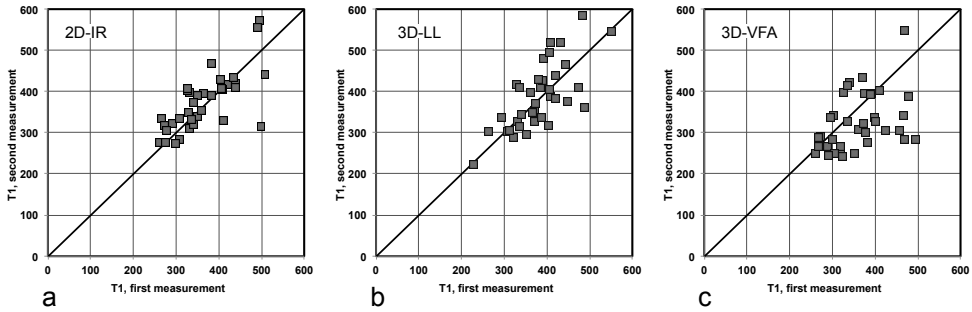

Figure 5.1 All first and second T_1 measurements with two week interval for nine subjects. Each subject comprises four markers in each diagram (anterior and posterior ROIs for lateral and medial condyles). Diagonals are reference lines. **a)** 2D-IR **b)** 3D-LL **c)** 3D-VFA

The repeatability is expressed by the root-mean-square coefficient of variation (CV_{RMS}) and the intraclass correlation coefficient (ICC) for each cartilage region (Atkinson, 1998).

Statistical analysis of the results suggest that the 2D-IR method has the best repeatability (CV_{RMS} ~7%, ICC ~0.7), closely followed by the 3D-LL method (CV_{RMS} ~7%, ICC ~0.6), as both methods showed high correlation between first and second measurements. The 3D-VFA method performed worse (CV_{RMS} ~11%, ICC >0.3), having very low correlation between the first and second measurements (compare to Fig. 5.1). The repeatability was roughly similar for all cartilage regions, both in medial and lateral condyles (**Paper II**).

It should be noted that the inferior results of the 3D-VFA method might be related to the lack of B_1 correction. In this study a transmitting extremity coil was used, which provides good SNR at the cost of more inhomogeneous B_1 field. If the later introduced B_1 correction method (**Paper III**) would have been used, the results might have been improved.

In repeated dGEMRIC measurements, variations to some degree are expected, due to the complexity of both the biological and technical processes involved. Part of this variation origins from different noise sensitivity for the measurement methods, as is illustrated by the results above. Another source of variation follows from the manual

outlining of the cartilage regions, as there will inevitably be variations when attempting to locate the exact same cartilage regions in images taken at different occasions.

Comparing the results of this study to similar studies in healthy cartilage (Multanen, 2009) reveals that the reported repeatability is about the same in both studies (**Paper II**). This finding suggest that dGEMRIC in early OA is not more fluctuant than in healthy cartilage. However, at a later stage of the disease, when the cartilage deterioration is worse, this conclusion might not be valid.

5.2 3D-LL dGEMRIC in the meniscus

The menisci play an important role as stabilizers and weight transmitters in the knee, primarily acting to redistribute contact forces across the tibiofemoral articulation (see section 2.2). Damages to the menisci can occur for a variety of reasons (e.g. trauma, age or disease), often resulting in tears that may affect the meniscal functionality, causing joint instability and increased stress on the cartilage (Beaufils, 2010). As a consequence, the menisci have gained increased attention since these factors are known to contribute in the development of OA (Neuman, 2008). Thus, being able to monitor meniscal health may both provide further clues in the understanding of OA as well as providing a model for studying early OA development.

The use of dGEMRIC in the meniscus is therefore an appealing alternative, which has not yet been widely explored. Prior to this work, only one full such study had been made, which concluded that degradation of adjacent cartilage is reflected by low T_1 in the meniscus, suggesting that some aspect of the molecular structure of the meniscus can be monitored by its T_1 value (Krishnan, 2007).

However, two additional studies were recently published in this field. In one of these, T_1-weighted signal intensity in meniscus is reported to have a peak at about three hours after contrast injection, suggesting this to be the optimal time point for meniscal dGEMRIC (Mayerhoefer, 2011). The other study concluded that the diagnostic value of the measured T_1 was similar regardless if an ionic or non-ionic contrast agent is used. This finding suggest that the retrieved T_1 value in meniscus is not primarily an effect of charge distribution, as it is assumed to be in articular cartilage (Li, 2011). Considering that the GAG concentration in the meniscus is almost an order of magnitude lower than it is in articular cartilage, this latter conclusion may very well hold true.

5.2.1 Time-response study

The previous meniscal studies have mostly been performed using dGEMRIC protocols optimized for articular cartilage. For this reason further investigation regarding contrast distribution kinetics in menisci is required, as the differences from articular cartilage include fundamental issues, such as parts of the menisci being vascular.

A time-response study was set up with 12 healthy subjects. ROIs were drawn in both vascular and avascular regions of the meniscus and also in the weight bearing parts of the femoral cartilage. T_1 measurements were performed both prior to contrast injection and at four time points after injection (at 60, 90, 120, and 180 minutes) (**Paper IV**). At each time point ΔR_1 was calculated, which is directly proportional to the concentration of contrast agent. This relates to the measured T1 value by

$$\Delta R_1 = \frac{1}{T_{1Gd}} - \frac{1}{T_{1pre}} \qquad \text{Eq. 5.1}$$

where $T_{1\text{pre}}$ and $T_{1\text{Gd}}$ are the measured T_1 values before and after contrast agent administration, respectively (compare to Eq. 2.1).

Due to very short T_2 within the meniscus, sequences with long echo time, such as 2D-IR, are not feasible as the signal fades away too quickly. With the 3D-LL sequence this is not an issue, due to its short echo time. Thus, in this study all T_1 measurements were performed using the 3D-LL sequence, evaluated with the precalculated flip angle correction method (**Paper I**).

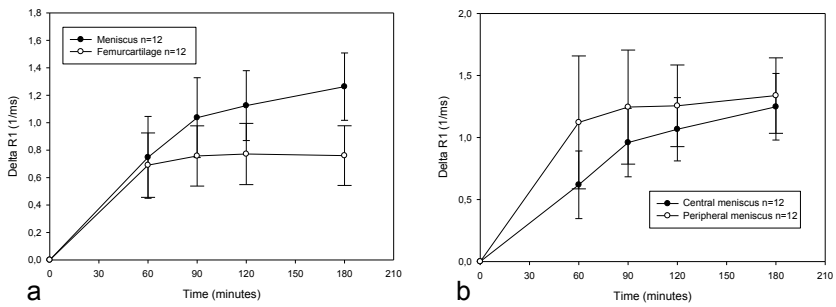

Figure 5.2 a) ΔR_1 at different time points following contrast agent administration, in the meniscus and femoral cartilage. **b)** ΔR_1 at different time points, in the central and peripheral parts of the posterior medial meniscus.

The main conclusions from this study is that there is indeed a contrast uptake in the meniscus, which seem to stagnate at about the same time as it does in the articular cartilage (Fig. 5.2a). This suggests that similar dGEMRIC timing is feasible for both articular cartilage and menisci (**Paper IV**).

It is also shown that the contrast uptake in the meniscus is much higher than in articular cartilage, which may relate to the considerably lower GAG concentration in the meniscus (**Paper IV**).

Analyzing the differences between regions of the menisci is associated with some uncertainties, due to the limited number of pixels within each region. However, in certain parts of the menisci such comparison was feasible (Fig. 5.2b), suggesting a faster contrast uptake in the vascular part of the meniscus (**Paper IV**).

At this stage it is to early to draw any extensive conclusions regarding the diagnostic value of using dGEMRIC in the meniscus. In particular, the method needs to be compared to similar studies of patients with damaged or diseased menisci, which is a planned next step in this project.

6. Summarized conclusions

In this thesis a series of 3D T_1 quantification methods have been developed and evaluated, primarily for assessment of cartilage quality using dGEMRIC.

A 3D Look-Locker (3D-LL) pulse sequence was first created. In order for the T_1 value to be correctly calculated throughout the entire volume, two novel methods were developed for correction of B_1 inhomogeneities and slab profile flip angle variations. To verify these methods, an *in vivo* knee-dGEMRIC study was set up at 1.5T to compare the results to gold standard 2D inversion recovery (2D-IR). One of the developed methods was shown to be sensitive to inversion pulse inaccuracies, making it unsuitable for *in vivo* usage. The other method performed well, generating very accurate *in vivo* results. (**Paper I**).

Next, a repeatability knee-dGEMRIC study was set up at 1.5T, in which a group of subjects at risk of developing OA were examined at two different occasions using three different T_1 quantification techniques. The 2D-IR and the 3D-LL sequences performed equally well, while the 3D variable flip angle (3D-VFA) sequence was inferior. Repeatability was shown to be similar to previously reported results in healthy subjects (**Paper II**).

This was followed by an investigation of the performance of 3D-VFA T_1 quantification in combination with a B_1 mapping sequence. The results with and without the B_1 mapping sequence was studied in hip-GEMRIC at both 1.5T and 3T. It was concluded that B_1 correction should always be used, especially at higher field strengths (**Paper III**).

Finally, a time-response study was performed at 1.5T to explore the feasibility of performing dGEMRIC in the menisci. The 3D-LL sequence was used for T_1 quantification. It was concluded that the temporal contrast uptake in the menisci follows that of the articular cartilage, but with higher contrast concentration. Differences in contrast uptake can also be seen between the vascular and the avascular parts of the menisci (**Paper IV**).

The overall conclusion of this work is that 3D T_1 quantification in dGEMRIC, with full B_1 correction, is definitely feasible and should allow for both new and improved means of diagnostics.

7. Future aspects

7.1 Improving the cartilage assessment

The search for the most optimal T_1 quantification sequence is far from over yet. Apart from turning to different sequences, there are room for improvements in both the 3D-LL and the 3D-VFA sequences.

Starting with the 3D-LL sequence, the preferred next step would be to incorporate additional means for *in vivo* mapping of the inversion pulse quality (variable K in Eq. 4.6) which in turn would make the local flip angle correction method feasible for clinical usage. This would be advantageous since it would allow for totally B_1 insensitive T_1 quantification. The mapping of the inversion quality could possibly be performed by running the 3D-LL sequence an additional time using different parameters, such as the delay time (TR-T_{Stop} in Fig. 4.5) being set to a minimum, allowing the K variable to be solved.

Regarding the 3D-VFA sequence, the B_1 correction could be combined with a precalculated flip angle slab profile (as in section 4.2.5). This would increase the T_1 accuracy in the outer parts of the slab, where the flip angle has dropped from its nominal value. A possible issue with this is that as the flip angle drops, it will no longer be optimal for T_1 quantification. However, this should not be a major issue.

In addition to the dGEMRIC technique, there are a few additional cartilage assessment techniques that should be further investigated. Of particular interest are gagCEST and sodium imaging, as both of these techniques aim to provide measurements that more directly correspond to the GAG level within the cartilage (see section 2.4.2). Setting up an initial comparative study between gagCEST and dGEMRIC is a prioritized next step, as that can be performed using ordinary 3T scanners with common clinical coils.

While the use of sodium cartilage imaging have been reported at 3T (Staroswiecki, 2010), it does require specialized coils and hardware configuration, making such studies more complicated than the other techniques. The low concentration of Na-ions will also pose a restriction on the acquired resolution, making sodium imaging generally more feasible for even higher magnetic field strengths. For this reason sodium imaging is not expected to be a major objective until a 7T scanner is available.

7.2 Automatic cartilage segmentation and 3D visualization

Although methods have been developed in this thesis for accurate T_1 quantification in a full 3D volume, the dGEMRIC data evaluation has been almost identical to that of the old 2D methods. While this is perfectly natural, considering that an important objective has been to compare the old 2D to the new 3D methods, the next step in the development will be to actually make use of the possibilities given by the 3D data.

In order to achieve this, automatic segmentation of the cartilage within the entire 3D volume will be required, as manual segmentations would be too time consuming. A significant amount of work have already been put into the initial development of such a method. Currently, the automatic segmentation is performed on T_1, T_2^* and proton density (PD) maps, simultaneously acquired using a slightly modified 3D-VFA sequence. The basic assumption is that the combined use of several parametric maps should allow for a maximized differentiation between tissues as well as a maximized diagnostic value. The additional use of a T_2 mapping DESPOT2 sequence (Deoni, 2003) will also be investigated.

The current segmentation method combines the parametric maps with an atlas based active shapes model for bone segmentation (Jain, 1996; Fripp, 2007) and a neural network model for cartilage identification (Long, 2010). Although the initial segmentation results are very promising, more research is needed until the method is working reliably within the entire 3D dataset. Once this is achieved, the segmented cartilage will allow for new means of visualization, for example in full 3D. As a diagnostic tool this might be powerful, since localized cartilage changes can then easily be seen and direct comparisons between different parts of the cartilage can be made.

The cartilage surfaces can also be normalized to anatomical landmarks, which should allow for simple inter-subject dGEMRIC comparisons over the entire cartilage volume. Such comparison may lead to new conclusions about cartilage diseases, since previous work has primarily been restricted to comparison of the weight-bearing regions within the cartilage.

The work is planned to be resumed following the dissertation and will be targeted towards the development of a complete cartilage evaluation software suite, intended for both research and clinical practice.

8. Afterword

The work behind this thesis started in the summer of 2006. During the years since then I have had the opportunity of being part of a dynamic research field, which has been a very inspiring experience.

Back in the year 2006, the dGEMRIC technique was already well-known with a plurality of available publications. At that time, classic 2D T_1 quantification were still the most commonly used techniques in dGEMRIC. The use of 3D techniques was at a very early stage, with not even a handful of published papers.

Inspired by the pioneering work by Kimelman et al, we decided to implement the 3D Look-Locker technique, since the reported preliminary dGEMRIC results seemed very promising. In the year 2007, we had this not only running, but also improved, by means of being able to directly correct for B_1 inhomogeneities. This work formed the basis for the first publication on which this thesis is based (**Paper I**).

Once the protocol was working reliably, other studies were initiated that made use of our newly developed technique. Among these were the repeatability study (**Paper II**) and the meniscus study (**Paper IV**), both started during the years 2008-2009.

At this time another 3D T_1 quantification technique had emerged and was gaining interest due to its simplicity to use. This was the 3D-VFA technique, which was released as a package that allowed the T_1 data to be evaluated directly on the scanner, instead of exporting it to a separate computer.

For this reason we decided to make our own implementation of the 3D-VFA technique, in order to be able to include it in our repeatability study and investigate its accuracy. The results were not in favor of the 3D-VFA technique (**Paper II**).

In the year 2010 the opportunity was given to spend a few months at Children's Hospital in Boston, where an updated beta version of the 3D-VFA sequence was available, now also including proper B_1 correction. The work in Boston aimed at evaluating the effects of this correction, resulting in the conclusion that the T_1 quantification accuracy of 3D-VFA had now been significantly improved (**Paper III**).

Today, both the 3D-LL and the 3D-VFA techniques suite the dGEMRIC needs well. Which one of the techniques to use is mostly a matter of choice. Following my dissertation on September 9, 2011, the next step in my continued research will be to explore the possibilities provided by the 3D dGEMRIC data.

9. Acknowledgements

Jag vill börja med att tacka min huvudhandledare Jonas Svensson för all support och vägledning under de här åren. Framförallt har jag uppskattat alla bra diskussioner som vi har haft och all den konstruktiva kritik som du har kommit med. Som handledare har du varit precis lagom närvarande, jag har kunnat bedriva mitt arbete på mitt eget sätt, men du har ändå lotsat mig i rätt riktning när det har behövts.

Jag vill också tacka mina båda andra handledare Leif Dahlberg och Sören Mattsson. Leif, tack för att du introducerat mig till ortopedivärlden. Att få synpunkter och kommentarer ur ett medicinskt perspektiv har verkligen varit värdefullt för mitt arbete, det är så lätt för en ingenjör att bara snöa in på det tekniska annars. Sören, tack för att du fångade in mig till radiofysikavdelningen från första början. Din förmåga att ordna lösningar på problem har varit ovärderlig.

Dessutom vill jag tacka Carl-Johan Tiderius, både för all hjälp med allting som varit broskrelaterat samt också för hjälpen med Bostonresan. Du har ju i princip också varit handledare för mig och alltid funnits där som ett bollplank när det har behövts.

I would also like to thank Dr. Young-Jo Kim at Children's Hospital in Boston for welcoming me into your research group for a period of time. I really enjoyed working for you and I am looking forward to have more collaboration with you in the future.

Stort tack även till Anetta och alla ni som arbetar vid magneterna. Inte bara har ni hjälpt oss att genomföra alla våra studier, ni har också haft tålamod när jag råkat krascha magneterna och sinkat era körscheman.

I would also like to thank my co-authors of the publications which form the basis of this thesis. Framförallt tack till Ulf Sigurdsson som är försteförfattare på Paper IV och därmed dragit det klart största lasset med denna.

Under den här tiden har jag lärt känna många människor som jag hoppas att jag kommer att fortsätta ha kontakt med. Tack hela radiofysikavdelningen för trevlig gemenskap. Tack MR-gruppen för givande samarbete. Tack alla doktorandkollegor för allt kul som vi har haft under dessa åren. Tack till mina rumskamrater, Sofie, Pernilla och Fredrik för alla bra diskussioner, youtubefilmer, fikapauser och annat som gjort att man sluppit jobba. Och ett synnerligt stort tack till den kakinköpsansvarige på radiofysikavdelningen för att det alltid funnits kakor i frysen!

Slutligen vill jag tacka vänner, släkt och familj. Framförallt tack Mamma och Pappa för att ni alltid har uppmuntrat mig i vad jag än har gjort och för att ni alltid ställer upp för mig. Och ett enormt stort tack till min Carina, inte bara för att du hjälpt mig och stöttat mig genom hela arbetet, men framförallt för att du är du.

Detta arbete har erhållit finansiellt stöd från Alfred Österlunds stiftelse, Greta och Johan Kocks stiftelser, Universitetssjukhuset MAS stiftelser och gåvor, Hulda och E Conrad Mossfelts stiftelse, O.E och Edla Johanssons vetenskapliga stiftelse, Magnus Bergvalls stiftelse samt Vetenskapsrådet.

10. References

Andreisek G, White L M, Yang Y, Robinson E, Cheng H L and Sussman M S (2009). "Delayed gadolinium-enhanced MR imaging of articular cartilage: three-dimensional T1 mapping with variable flip angles and B1 correction", Radiology 252(3): 865-873.

Atkinson G and Nevill A M (1998). "Statistical methods for assessing measurement error (reliability) in variables relevant to sports medicine", Sports Med 26(4): 217-238.

Bashir A, Gray M L and Burstein D (1996). "Gd-DTPA2- as a measure of cartilage degradation", Magn Reson Med 36(5): 665-673.

Bashir A, Gray M L, Hartke J and Burstein D (1999). "Nondestructive imaging of human cartilage glycosaminoglycan concentration by MRI", Magn Reson Med 41(5): 857-865.

Beaufils P and Verdonk R (2010). "The Meniscus", Springer Verlag.

Bellamy N (2002). "WOMAC Osteoarthritis Index User Guide. Version V.", Brisbane, Australia.

Bernstein M A, King K F and Zhou X J (2004). "Handbook of MRI Pulse Sequences", London, Academic Press Inc.

Braun S, Steadman J R, Rodkey W G and Briggs K K (2008). "Mikrofrakturierung und spezifische Rehabilitation zur Behandlung von Arthrose des Kniegelenks", Arthroskopie 22(3): 183-192.

Brix G, Schad L R, Deimling M and Lorenz W J (1990). "Fast and precise T1 imaging using a TOMROP sequence", Magn Reson Imaging 8(4): 351-356.

Brookes J A, Redpath T W, Gilbert F J, Murray A D and Staff R T (1999). "Accuracy of T1 measurement in dynamic contrast-enhanced breast MRI using two- and three-dimensional variable flip angle fast low-angle shot", J Magn Reson Imaging 9(2): 163-171.

Burstein D, Velyvis J, Scott K T, Stock K W, Kim Y J, Jaramillo D, . . . Gray M L (2001). "Protocol issues for delayed Gd(DTPA)(2-)-enhanced MRI (dGEMRIC) for clinical evaluation of articular cartilage", Magn Reson Med 45 (1): 36-41.

Carlson J W and Kramer D M (1990). "Rapid radiofrequency calibration in MRI", Magn Reson Med 15(3): 438-445.

Deichmann R and Haase A (1991). "Quantification of Tl Values by SNAPSHOT-FLASH NMR Imaging", Journal of Magnetic Resonance (96): 5.

Deoni S C, Peters T M and Rutt B K (2004). "Determination of optimal angles for variable nutation proton magnetic spin-lattice, T1, and spin-spin, T2, relaxation times measurement", Magn Reson Med 51(1): 194-199.

Deoni S C, Rutt B K and Peters T M (2003). "Rapid combined T1 and T2 mapping using gradient recalled acquisition in the steady state", Magn Reson Med 49(3): 515-526.

Donnan F G (1924). "The theory of membrane equilibria", Chem Rev: 1:73–90.

Eckstein F, Ateshian G, Burgkart R, Burstein D, Cicuttini F, Dardzinski B, . . . Felson D (2006). "Proposal for a nomenclature for magnetic resonance imaging based measures of articular cartilage in osteoarthritis", Osteoarthritis Cartilage 14(10): 974-983.

Ericsson Y B, Tjornstrand J, Tiderius C J and Dahlberg L E (2009). "Relationship between cartilage glycosaminoglycan content (assessed with dGEMRIC) and OA risk factors in meniscectomized patients", Osteoarthritis Cartilage 17(5): 565-570.

Ernst R and Anderson W (1966). "Application of Fourier Transform Spectroscopy to Magnetic Resonance", Rev. Sci. Instr. 37: 93-102.

Fripp J, Crozier S, Warfield S K and Ourselin S (2007). "Automatic segmentation of the bone and extraction of the bone-cartilage interface from magnetic resonance images of the knee", Phys Med Biol 52(6): 1617-1631.

Gowland P A and Stevenson V L (2004). "T1: the Longitudinal Relaxation Time" in Tofts P (Ed.) "Quantitative MRI of the Brain: Measuring Changes Caused by Disease".

Gray H and Lewis W (1918). "Anatomy of the human body, by Henry Gray. 20th ed.", Philadelphia, Lea & Febiger.

Gupta R, Feretti J, Becker E and Weiss G (1980). "A Modified Fast Inversion-Recovery Technique for Spin-Lattice Relaxation Measurements", Journal of Magnetic Resonance 38: 447-452.

Haacke E M (1999). "Magnetic resonance imaging: physical principles and sequence design", J. Wiley & Sons.

Henderson E, McKinnon G, Lee T Y and Rutt B K (1999). "A fast 3D look-locker method for volumetric T1 mapping", Magn Reson Imaging 17(8): 1163-1171.

Hinson W H and Sobol W T (1988). "A new method of computing spin-lattice relaxation maps in magnetic resonance imaging using fast scanning protocols", Med Phys 15(4): 551-561.

Homer J and Beevers M (1985). "Driven-equilibrium single-pulse observation of T1 relaxation. A re-evaluation of a rapid 'new' method for determining NMR spin-lattice relaxation times.", J Magn Reson 63: 287-297.

Hornak J P, Szumowski J and Bryant R G (1988). "Magnetic field mapping", Magn Reson Med 6(2): 158-163.

Jain A, Yu Z and Lakshmanan S (1996). "Object matching using deformable templates", Pattern Analysis and Machine Intelligence 18(3): 267 - 278.

Kellgren J H and Lawrence J S (1957). "Radiological assessment of osteo-arthrosis", Ann Rheum Dis 16(4): 494-502.

Kimelman T, Vu A, Storey P, McKenzie C, Burstein D and Prasad P (2006). "Three-dimensional T1 mapping for dGEMRIC at 3.0 T using the Look Locker method", Invest Radiol 41(2): 198-203.

King D (1936). "The healing of semilunar cartilage", J Bone Joint Surg 18: 333–342.

Kingsley P B, Ogg R J, Reddick W E and Steen R G (1998). "Correction of errors caused by imperfect inversion pulses in MR imaging measurement of T1 relaxation times", Magn Reson Imaging 16(9): 1049-1055.

Koopman W J (1997). "Arthritis and allied conditions: a textbook of rheumatology", Williams & Wilkins.

Krishnan N, Shetty S K, Williams A, Mikulis B, McKenzie C and Burstein D (2007). "Delayed gadolinium-enhanced magnetic resonance imaging of the meniscus: an index of meniscal tissue degeneration?", Arthritis Rheum 56(5): 1507-1511.

Lai W M, Hou J S and Mow V C (1991). "A triphasic theory for the swelling and deformation behaviors of articular cartilage", J Biomech Eng 113(3): 245-258.

Lammentausta E, Frank E, Hawezi Z, Grodzinsky A and Dahlberg L (2011). "Contrast agent diffusion in dGEMRIC: exploring Donnan equlibrium in vitro and in vivo", Abstract at International Society for Magnetic Resonance in Medicine (ISMRM) meeting, Montreal, Canada.

Levenberg K (1944). "A Method for the Solution of Certain Non-linear Problems in Least-Squares", Quarterly of Applied Mathematics 2(2): 5.

Li W, Du H, Scheidegger R, Wu Y and Prasad P V (2009). "Value of precontrast T(1) for dGEMRIC of native articular cartilage", J Magn Reson Imaging 29(2): 494-497.

Li W, Edelman R R and Prasad P V (2011). "Delayed contrast enhanced MRI of meniscus with ionic and non-ionic agents", J Magn Reson Imaging 33(3): 731-735.

Li W, Scheidegger R, Wu Y, Edelman R R, Farley M, Krishnan N, . . . Prasad P V (2010). "Delayed contrast-enhanced MRI of cartilage: comparison of nonionic and ionic contrast agents", Magn Reson Med 64(5): 1267-1273.

Li W, Scheidegger R, Wu Y, Vu A and Prasad P V (2008). "Accuracy of T1 measurement with 3-D Look-Locker technique for dGEMRIC", J Magn Reson Imaging 27(3): 678-682.

Ling W, Regatte R R, Navon G and Jerschow A (2008). "Assessment of glycosaminoglycan concentration in vivo by chemical exchange-dependent saturation transfer (gagCEST)", Proc Natl Acad Sci U S A 105(7): 2266-2270.

Lohmander L S, Englund P M, Dahl L L and Roos E M (2007). "The long-term consequence of anterior cruciate ligament and meniscus injuries: osteoarthritis", Am J Sports Med 35(10): 1756-1769.

Long N Q, Jiang D and Ding C (2010). "Application of Artificial Neural Networks in Automatic Cartilage Segmentation", Third International Workshop on Advanced Computational Intelligence, Suzhou, Jiangsu, China.

Look and Locker (1970). "Time saving in measurement of NMR and EPR relaxation times", Rev. Sci. Instr. 41(2): 250-251.

Lusse S, Claassen H, Gehrke T, Hassenpflug J, Schunke M, Heller M and Gluer C C (2000). "Evaluation of water content by spatially resolved transverse relaxation times of human articular cartilage", Magn Reson Imaging 18(4): 423-430.

Mamisch T C, Dudda M, Hughes T, Burstein D and Kim Y J (2008). "Comparison of delayed gadolinium enhanced MRI of cartilage (dGEMRIC) using inversion recovery and fast T1 mapping sequences", Magn Reson Med 60(4): 768-773.

Manuel A, Li W, Jellus V, Hughes T and Prasad P V (2011). "Variable flip angle-based fast three-dimensional T1 mapping for delayed gadolinium-enhanced MRI of cartilage of the knee: need for B1 correction", Magn Reson Med 65(5): 1377-1383.

Marquardt D (1963). "An Algorithm for the Least-Squares Estimation of Nonlinear Parameters", SIAM Journal of Applied Mathematics 11(2): 11.

Mayerhoefer M E, Mamisch T C, Riegler G, Welsch G H, Dobrocky T, Weber M, . . . Trattnig S (2011). "Gadolinium diethylenetriaminepentaacetate enhancement kinetics in the menisci of asymptomatic subjects: a first step towards a dedicated dGEMRIC (delayed gadolinium-enhanced MRI of cartilage)-like protocol for biochemical imaging of the menisci", NMR Biomed.

McDermott I D, Masouros S D, Bull A M J and Amis A A (2010). "Anatomy" in Beaufils P and Verdonk R (Eds). "The Meniscus", Springer Verlag.

Menezes N M, Gray M L, Hartke J R and Burstein D (2004). "T2 and T1rho MRI in articular cartilage systems", Magn Reson Med 51(3): 503-509.

Mow V, Ateshian G, Lai W, Sun D, Wang C and Gu W (1989). "Effects of fixed charge density on the stress-relaxation behavior of hydrated soft tissues in confined compression", Int J Solids Structures 35: 4945–4962.

Mow V, Kuei S, Lai W and Armstrong C (1980). "Biphasic creep and stress relaxation of articular cartilage in compression? Theory and experiments", J Biomech Eng 102: 73–84.

Mow V C, Gu W Y and Chen F H (2005). "Structure and Function of Articular Cartilage and Meniscus " in Mow V C and Huiskes R (Eds). "Basic orthopaedic biomechanics & mechano-biology", Lippincott Williams & Wilkins.

Mow V C and Hung T H (2001). "Biomechanics of Articular Cartilage" in Nordin M and Frankel V H (Eds). "Basic biomechanics of the musculoskeletal system", Lippincott Williams & Wilkins.

Multanen J, Rauvala E, Lammentausta E, Ojala R, Kiviranta I, Hakkinen A, . . . Heinonen A (2009). "Reproducibility of imaging human knee cartilage by delayed gadolinium-enhanced MRI of cartilage (dGEMRIC) at 1.5 Tesla", Osteoarthritis Cartilage 17(5): 559-564.

Murata M, Yudoh K and Masuko K (2008). "The potential role of vascular endothelial growth factor (VEGF) in cartilage: how the angiogenic factor could be involved in the pathogenesis of osteoarthritis?", Osteoarthritis Cartilage 16 (3): 279-286.

Neuman P, Englund M, Kostogiannis I, Friden T, Roos H and Dahlberg L E (2008). "Prevalence of tibiofemoral osteoarthritis 15 years after nonoperative treatment of anterior cruciate ligament injury: a prospective cohort study", Am J Sports Med 36(9): 1717-1725.

Nieminen M T, Rieppo J, Toyras J, Hakumaki J M, Silvennoinen J, Hyttinen M M, . . . Jurvelin J S (2001). "T2 relaxation reveals spatial collagen architecture in articular cartilage: a comparative quantitative MRI and polarized light microscopic study", Magn Reson Med 46(3): 487-493.

Nieminen M T, Toyras J, Laasanen M S, Silvennoinen J, Helminen H J and Jurvelin J S (2004). "Prediction of biomechanical properties of articular cartilage with quantitative magnetic resonance imaging", J Biomech 37(3): 321-328.

Nuki G (1999). "Osteoarthritis: a problem of joint failure", Z Rheumatol 58(3): 142-147.

Oh C H, Hilal S K, Cho Z H and Mun I K (1990). "Radio frequency field intensity mapping using a composite spin-echo sequence", Magn Reson Imaging 8(1): 21-25.

Outerbridge R E (1961). "The etiology of chondromalacia patellae", J Bone Joint Surg Br 43-B: 752-757.

Owman H, Tiderius C J, Neuman P, Nyquist F and Dahlberg L E (2008). "Association between findings on delayed gadolinium-enhanced magnetic resonance imaging of cartilage and future knee osteoarthritis", Arthritis Rheum 58(6): 1727-1730.

Parker D A, Trivett A J and Amendola A (2008). "Technique in high tibial osteotomy" in Bonnin M and Chambat P (Eds). "Osteoarthrisis of the Knee", Springer.

Perman W H, Bernstein M A and Sandstrom J C (1989). "A method for correctly setting the rf flip angle", Magn Reson Med 9(1): 16-24.

Reddy R, Li S, Noyszewski E A, Kneeland J B and Leigh J S (1997). "In vivo sodium multiple quantum spectroscopy of human articular cartilage", Magn Reson Med 38(2): 207-214.

Regatte R R, Akella S V, Borthakur A, Kneeland J B and Reddy R (2002). "Proteoglycan depletion-induced changes in transverse relaxation maps of cartilage: comparison of T2 and T1rho", Acad Radiol 9(12): 1388-1394.

Roos E M, Roos H P, Lohmander L S, Ekdahl C and Beynnon B D (1998). "Knee Injury and Osteoarthritis Outcome Score (KOOS)--development of a self-administered outcome measure", J Orthop Sports Phys Ther 28(2): 88-96.

Schmitt B, Zbyn S, Stelzeneder D, Jellus V, Paul D, Lauer L, . . . Trattnig S (2011). "Cartilage Quality Assessment using gagCEST and Sodium MRI at 7 Tesla", Abstract at International Society for Magnetic Resonance in Medicine (ISMRM) meeting, Montreal, Canada.

Sepponen R E, Pohjonen J A, Sipponen J T and Tanttu J I (1985). "A method for T1 rho imaging", J Comput Assist Tomogr 9(6): 1007-1011.

Siversson C, Tiderius C J, Dahlberg L and Svensson J (2009). "B1 inhomogeneity corrected T1-quantification for dGEMRIC using 3D Look-Locker technique with non-slice selective RF-pulses", Abstract at International Society for Magnetic Resonance in Medicine (ISMRM) meeting, Honolulu, Hawaii: 6659.

Siversson C, Tiderius C J, Dahlberg L and Svensson J (2009). "Gradient Echo assisted 3D Look-Locker - A method for improved volume T1-quantification accuracy applied to dGEMRIC", Abstract at International Society for Magnetic Resonance in Medicine (ISMRM) meeting, Honolulu, Hawaii: 6659.

Sommerlath K and Hamberg P (1989). "Healed meniscal tears in unstable knees. A long-term followup of seven years", Am J Sports Med 17(2): 161-163.

Stanisz G J and Henkelman R M (2000). "Gd-DTPA relaxivity depends on macromolecular content", Magn Reson Med 44(5): 665-667.

Staroswiecki E, Bangerter N K, Gurney P T, Grafendorfer T, Gold G E and Hargreaves B A (2010). "In vivo sodium imaging of human patellar cartilage with a 3D cones sequence at 3 T and 7 T", J Magn Reson Imaging 32(2): 446-451.

Stollberger R and Wach P (1996). "Imaging of the active B1 field in vivo", Magn Reson Med 35(2): 246-251.

Tiderius C, Hori M, Williams A, Sharma L, Prasad P V, Finnell M, . . . Burstein D (2006). "dGEMRIC as a function of BMI", Osteoarthritis Cartilage 14(11): 1091-1097.

Tiderius C J, Jessel R, Kim Y J and Burstein D (2007). "Hip dGEMRIC in asymptomatic volunteers and patients with early osteoarthritis: the influence of timing after contrast injection", Magn Reson Med 57(4): 803-805.

Tiderius C J, Olsson L E, de Verdier H, Leander P, Ekberg O and Dahlberg L (2001). "Gd-DTPA2- enhanced MRI of femoral knee cartilage: a dose-response study in healthy volunteers", Magn Reson Med 46(6): 1067-1071.

Tiderius C J, Olsson L E, Leander P, Ekberg O and Dahlberg L (2003). "Delayed gadolinium-enhanced MRI of cartilage (dGEMRIC) in early knee osteoarthritis", Magn Reson Med 49(3): 488-492.

Tiderius C J, Svensson J, Leander P, Ola T and Dahlberg L (2004). "dGEMRIC (delayed gadolinium-enhanced MRI of cartilage) indicates adaptive capacity of human knee cartilage", Magn Reson Med 51(2): 286-290.

Tiderius C J, Tjornstrand J, Akeson P, Sodersten K, Dahlberg L and Leander P (2004). "Delayed gadolinium-enhanced MRI of cartilage (dGEMRIC): intra- and interobserver variability in standardized drawing of regions of interest", Acta Radiol 45(6): 628-634.

Tofts P, Ed. (2004). "Quantitative MRI of the Brain: Measuring Changes Caused by Disease", Hoboken, NJ, John Wiley & Sons, Ltd.

Trattnig S, Marlovits S, Gebetsroither S, Szomolanyi P, Welsch G H, Salomonowitz E, . . . Mamisch T C (2007). "Three-dimensional delayed gadolinium-enhanced MRI of cartilage (dGEMRIC) for in vivo evaluation of reparative cartilage after matrix-associated autologous chondrocyte transplantation at 3.0T: Preliminary results", J Magn Reson Imaging 26(4): 974-982.

van der Meulen P, Groen J P, Tinus A M and Bruntink G (1988). "Fast Field Echo imaging: an overview and contrast calculations", Magn Reson Imaging 6(4): 355-368.

Verdonk P (2010). "Histology-Ultrastructure-Biology" in Beaufils P and Verdonk R (Eds). "The Meniscus", Springer Verlag.

Walker P S and Erkman M J (1975). "The role of the menisci in force transmission across the knee", Clin Orthop Relat Res (109): 184-192.

Watanabe A, Wada Y, Obata T, Ueda T, Tamura M, Ikehira H and Moriya H (2006). "Delayed gadolinium-enhanced MR to determine glycosaminoglycan concentration in reparative cartilage after autologous chondrocyte implantation: preliminary results", Radiology 239(1): 201-208.

Wheaton A J, Casey F L, Gougoutas A J, Dodge G R, Borthakur A, Lonner J H, . . . Reddy R (2004). "Correlation of T1rho with fixed charge density in cartilage", J Magn Reson Imaging 20(3): 519-525.

WHO (2002)."The World Health Report".

Williams A, Mikulis B, Krishnan N, Gray M, McKenzie C and Burstein D (2007). "Suitability of T(1Gd) as the dGEMRIC index at 1.5T and 3.0T", Magn Reson Med 58(4): 830-834.

Yarnykh V L (2007). "Actual flip-angle imaging in the pulsed steady state: a method for rapid three-dimensional mapping of the transmitted radiofrequency field", Magn Reson Med 57(1): 192-200.

Yen Y M, Cascio B, O'Brien L, Stalzer S, Millett P J and Steadman J R (2008). "Treatment of osteoarthritis of the knee with microfracture and rehabilitation", Med Sci Sports Exerc 40(2): 200-205.

Zheng S and Xia Y (2010). "The impact of the relaxivity definition on the quantitative measurement of glycosaminoglycans in cartilage by the MRI dGEMRIC method", Magn Reson Med 63(1): 25-32.

Paper I

[redacted]

Original Research

Local Flip Angle Correction for Improved Volume T1-Quantification in Three-Dimensional dGEMRIC Using the Look-Locker Technique

Carl Siversson, MS,[1*] Carl-Johan Tiderius, MD, PhD,[2] Leif Dahlberg, MD, PhD,[2] and Jonas Svensson, PhD[1]

Purpose: To present an evaluation method for three-dimensional Look-Locker (3D-LL) based T1 quantification, calculating correct T1 values independent of local flip angle (FA) variations. The method was evaluated both in phantoms and in vivo in a delayed Gadolinium Enhanced MRI of Cartilage (dGEMRIC) study with 33 subjects.

Materials and Methods: T1 was measured with 3D-LL, using both local FA correction and a precalculated FA slice profile, and compared with standard constant FA correction, for all slices in phantoms and in both femur condyles in vivo. T1 measured using two-dimensional Inversion Recovery (2D-IR) was used as gold standard.

Results: Due to the FA being slice dependent, the standard constant FA correction results in erroneous T1 (systematic error = 109.1 ms in vivo), especially in the outer slices. With local FA correction, the calculated T1 is excellent for all slices in phantoms (<5% deviation from 2D-IR). In vivo the performance is lower (systematic error = −57.5 ms), probably due to imperfect inversion. With precalculated FA correction the performance is very good also in vivo (systematic error = 13.3 ms).

Conclusion: With the precalculated FA correction method, the 3D-LL sequence is robust enough for in vivo dGEMRIC, even outside the centermost slices.

Key Words: Look-Locker; T1 mapping; flip angle correction; B1 correction; dGEMRIC; cartilage
J. Magn. Reson. Imaging 2009;30:834–841.

OSTEOARTHRITIS (OA) is a common long-term disease characterized by loss and degradation of cartilage, causing severe pain and dysfunctionality, primarily in high-load joints such as the knees. In several previous studies (1–4), a method for early disease evaluation of OA has been presented. This method, known as delayed Gadolinium Enhanced MRI of Cartilage (dGEMRIC), provides an estimation of the glycosaminoglycan (GAG) content in the cartilage, which is known to be decreased at early stages of OA. The technique is based on the principle that the negatively charged contrast agent $Gd(DTPA)^{2-}$ (Magnevist, Berlex, Wayne, NJ), distributes in the cartilage in an inverse relationship to the GAG content. In normal cartilage, $Gd(DTPA)^{2-}$ is repelled by the abundant negatively charged GAG, whereas in conditions of GAG loss, more $Gd(DTPA)^{2-}$ will be distributed within the cartilage matrix. When the intravenously injected contrast agent has approximately reached its peak concentration in the cartilage, a quantitative measurement of T1 in the cartilage is performed, which will then correlate to the distributed amount of $Gd(DTPA)^{2-}$. Hence, longer T1 corresponds to higher cartilage quality and vice versa.

Traditionally dGEMRIC has been performed using a two-dimensional T1-quantifying Inversion Recovery (2D-IR) sequence (1,2,4). Recently, however, several methods for performing dGEMRIC in a three-dimensional (3D) volume of interest have emerged. These are based on various techniques such as Inversion Recovery prepared Spoiled Gradient Echo (5) (3D-IR SPGR), Look-Locker (6) (3D-LL), and 2-point Variable Flip Angle (7) (3D-VFA).

There are several advantages of using such 3D measurements, including improved possibilities for giving diagnoses regarding specific locations on the cartilage as well as improved possibilities for performing measurements that can more easily be reproduced.

Both the 3D-LL and the 3D-VFA techniques rely on a well-defined flip angle to obtain reliable measurements. A problem with this approach is that the flip angle is usually not very accurate outside of the centermost slices of the volume of interest, due to the radio frequency (RF) pulse excitation profile being nonrectangular. This typically renders erroneous T1 values outside of these slices, which limits the usefulness of such 3D measurement techniques. Local flip angle variations may also be caused by B1-inhomogeneities, further reducing the accuracy of the T1-measurements. While the 3D-IR SPGR does not suffer from these particular

[1]Department of Radiation Physics, Lund University, Malmö, Sweden.
[2]Department of Orthopedics, Lund University, Malmö, Sweden.
*Address reprint requests to: C.S., Department of Radiation Physics, Malmö University Hospital, SE-205 02 Malmö, Sweden. E-mail: carl.siversson@med.lu.se
Received January 19, 2009; Accepted July 8, 2009.
DOI 10.1002/jmri.21906
Published online in Wiley InterScience (www.interscience.wiley.com).

problems, it does instead suffer from long measurement times, typically twice that of other 3D sequences, which limits its usefulness for in vivo studies.

Brix et al (8) have previously suggested a method for correcting for flip angle inhomogeneities within a 2D Look-Locker image, by calculating the effect of each single excitation pulse and by taking all moments of free relaxation before, during and after the pulse train into account. For other related T1 measurement techniques, other ways of correcting for flip angle variations have been suggested (9), these, however, usually require additional sequences, which extends the total measurement time.

The aim of this study is to present and test an evaluation method for 3D dGEMRIC data, based on the 3D Look-Locker pulse sequence, performing a local flip angle correction, for calculation of correct T1 values throughout all slices and positions in the volume of interest, without adding additional pulse sequences. The improvement in T1 quantification accuracy compared with conventional 3D Look-Locker data is evaluated using 2D Inversion Recovery as gold standard. Evaluation is performed in phantoms as well as in vivo.

MATERIALS AND METHODS

The 3D Look-Locker Pulse Sequence

The 3D Look-Locker sequence used in this study is based on the sequence described by Henderson et al (10), which in turn is based on the work by Look and Locker (11). A slice-selective adiabatic inversion pulse is applied followed by a train of low flip angle excitation pulses, separated by a small time t_f, to repeatedly sample the recovery of the longitudinal magnetization using a gradient echo. Remaining transversal magnetization is destroyed between the excitation pulses by means of RF and gradient spoiling.

By encoding each group of n successive gradient echoes into one of m separate k-spaces, a total of m separate set of image volumes are generated, each representing a specific temporal position (i.e., inversion time, TI) along the longitudinal relaxation curve. For each group of n successive gradient echoes, the entire slice direction encodings are acquired using a linear encoding scheme. The process is repeated for new inversion pulses until all k-spaces are fully encoded. The actual TI for each image volume c ($1 \leq c \leq m$) is thus given by $TI_c = T_{start} + (c\text{-}1) \cdot n \cdot t_f + 0.5 \cdot n \cdot t$, where T_{start} is the time of the first excitation pulse, which is usually chosen as short as possible with respect to crusher gradients following the inversion pulse.

The signal $S(c)$ for a voxel in a given image volume c is proportional to the magnetization $M(TI_c)$ in the same voxel for the corresponding TI_c. This can be described by Eq. [1], where $T1^*$ is the apparent longitudinal relaxation time, and M_B and M_A are the extrapolated initial and steady-state longitudinal magnetization values respectively. By performing a three-parameter least square fit, using signal data from all image volumes, the parameters $T1^*$, M_B, and M_A can be estimated for each voxel.

$$S(c) \propto (TI_c) = M_A - (M_A - M_B) \cdot e^{-\frac{TI_c}{T1^*}} \qquad [1]$$

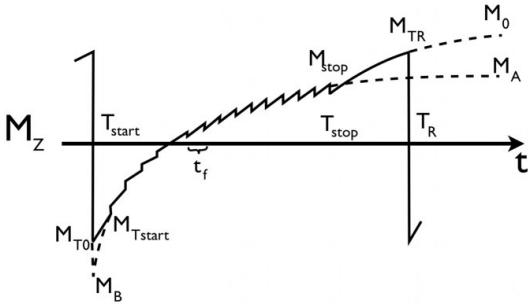

Figure 1. The complete longitudinal magnetization evaluation throughout one repetition in a Look-Locker sequence. An inversion pulse is applied, followed by a train of low flip angle excitation pulses, starting at T_{start} and continuing until T_{stop}. The corresponding longitudinal magnetizations are thus M_{Tstart} and M_{Tstop}. The excitation pulses are separated by a short time t_f. Variables M_A and M_B, together with the apparent time constant T1*, are retrieved from a three-parameter curve fit. Before and after the pulse train are short durations of undisturbed relaxation, evaluating toward M_0 with the true time constant T1, starting from M_{T0} and M_{Tstop}, respectively. At the time TR a new inversion pulse is applied and the relaxation cycle is repeated.

Because the recovery of the magnetization is affected by the applied RF pulses, the resulting $T1^*$ is shorter than the true $T1$. Thus, the calculation of the true $T1$ is dependent on the excitation pulse flip angle, which must be properly corrected for. Following are three different approaches on how to perform such correction.

Constant Flip Angle Correction

This is the correction technique traditionally used with both 2D and 3D Look-Locker sequences. It has been previously described (8,10) that the resulting $T1^*$ can be corrected using equation 2.

$$\frac{1}{T_1} = \frac{1}{T_1^*} + \frac{\ln(\cos(\alpha))}{t_f} \qquad [2]$$

However, one major drawback of this approach is that it requires the flip angle, α, to be well determined in every voxel being corrected. Commonly, the nominal flip angle from the user interface is used for all voxels and hence we refer to this method as constant flip angle (FA) correction.

Local Flip Angle Correction

With constant FA correction, not all of the available information about the magnetization evaluation is used. However, by taking several more of the variables affecting the longitudinal magnetization into account, an alternative method can be derived. The method we present here performs a local correction of $T1^*$, without a priori knowledge of the actual flip angle.

The longitudinal magnetization evaluation throughout one repetition in a 3D Look-Locker sequence is shown in Figure 1. The variables M_A, M_B, and $T1^*$ can be

retrieved using a three-parameter fit of Eq. [1], as described above. After the second repetition (T_R) the magnetization will have reached an equilibrium satisfying $M_{T0} = K \cdot M_{TR}$, where K is the quality of the inversion pulse ($0 \leq K \leq 1$).

The relationship between M_0 and M_A is established by the well-known longitudinal steady state function for a spoiled gradient echo (12) in Eq. [3].

$$M_A \cdot \left(1 - e^{-\frac{t_f}{T_1}} \cdot \cos(\alpha)\right) = M_0 \cdot \left(1 - e^{-\frac{t_f}{T_1}}\right) \quad [3]$$

By combining this relationship with Eq. [2], it is possible to derive Eq. [4], which describes the true *T1* as a function of several parameters of which only M_0 is unknown.

$$T_1 = -\frac{t_f}{\ln\left(1 - \frac{M_A - M_A \cdot e^{-\frac{t_f}{T_1^*}}}{M_0}\right)} \quad [4]$$

To calculate M_0 it is necessary to set up relations describing the magnetization levels at the start and the stop of the pulse train (M_{Tstart} and M_{Tstop} at times T_{start} and T_{stop}). These levels are easily calculated using the fitted parameters *T1**, M_A, and M_B, as shown in Eqs. [5] and [6].

$$M_{Tstart} = M_A - (M_A - M_B) \cdot e^{-\frac{T_{start}}{T_1^*}} \quad [5]$$

$$M_{Tstop} = M_A - (M_A - M_B) \cdot e^{-\frac{T_{stop}}{T_1^*}} \quad [6]$$

It is also possible to describe these magnetization levels as points in one of the undisturbed relaxation processes occurring before and after the pulse train, which are both evolving toward M_0. This is shown in Eqs. [7] and [8].

$$M_{Tstart} = M_0 - (M_0 - M_{T0}) \cdot e^{-\frac{T_{start}}{T_1}} \quad [7]$$

$$M_{TR} = M_0 - (M_0 - M_{Tstop}) \cdot e^{-\frac{T_R - T_{stop}}{T_1}} \quad [8]$$

By combining the equations of the undisturbed relaxation processes (Eqs. [7] and [8]) with the known variables M_{Tstart} and M_{Tstop} (Eqs. [5] and [6]) together with the expression for the inversion quality, Eq. [9] is retrieved, solving the previously unknown M_0.

$$M_0 = \frac{M_{Tstart} + M_{Tstop} \cdot K \cdot e^{-\frac{T_{start}}{T_1}} \cdot e^{-\frac{T_R - T_{stop}}{T_1}}}{1 - e^{-\frac{T_{start}}{T_1}} - K \cdot e^{-\frac{T_{start}}{T_1}} + K \cdot e^{-\frac{T_{start}}{T_1}} \cdot e^{-\frac{T_R - T_{stop}}{T_1}}} \quad [9]$$

By combining and solving equations 4 and 9, using an arithmetical or numerical method, the true T1 and M_0 for the current voxel can be calculated without knowledge of the actual flip angle, assuming that the inversion quality K is known or can be estimated. This method is thus referred to as local flip angle (FA) correction.

The numerical method to solve Eqs. [4] and [9] could be an iterative procedure, in which an initial *T1 = T1** is used as input to Eq. [9], yielding an M_0 which in turn is used as input to Eq. [4]. The resulting *T1* from Eq. [4] is in turn used as input for Eq. [9] again, and the process iterates until the calculated *T1* has converged toward a value not changing significantly between successive iterations.

Precalculated Flip Angle Correction

With the local FA correction method, the parameter describing the inversion quality, K, is still unresolved from Eqs. [4] and [9]. Depending on the type of inversion pulse used and the physical properties of the investigated sample, it may or may not be possible to perform a proper estimation of this parameter.

If the inversion quality cannot be properly estimated, it will be necessary to calculate the true flip angle in each region of interest by other means. The acquired *T1** for each region of interest can then be corrected using this calculated flip angle in combination with Eq. [2].

If it can be assumed that the major source for flip angle variations within a sample is due to the shape of the RF-pulse excitation profile, the variations in flip angle will be mostly slice dependent. Thus, by calculating a flip angle slice profile, the acquired T1* can be effectively corrected knowing only the slice origin for the corresponding region of interest.

By first executing the Look-Locker sequence in an environment where the inversion quality is well defined, a flip angle slice profile can be created. This slice profile will then be valid for correction of any other Look-Locker data acquired using the exact same excitation pulse, regardless of the quality of the inversion. This method is referred to as precalculated FA correction.

The flip angle is calculated by rewriting Eq. [2] as Eq. [10] and inserting the T1 value acquired using the local FA correction method in combination with the corresponding T1*.

$$\alpha = \arccos\left(e^{t_f\left(\frac{1}{T_1} - \frac{1}{T_1^*}\right)}\right) \quad [10]$$

MR Acquisition

All data were acquired on a 1.5 Tesla Siemens Sonata whole-body scanner (Siemens Medical Systems, Erlangen, Germany) using a transmit-receive CP-Extremity coil. T1 was measured using a standard 2D inversion recovery (2D-IR) pulse sequence and an in-house developed 3D Look-Locker (3D-LL) pulse sequence. The T1-evaluations for the 2D-IR were performed using the MRIMapper software developed at the Beth Israel Deaconess Medical Center (Boston, MA). The T1-evaluations for the 3D-LL sequence were performed using custom in-house developed software, which was programmed in Matlab (The Mathworks Inc, Natick, MA).

For 2D-IR the same sequence was repeated six times using different TI (50, 100, 200, 400, 800, and 1600 ms). The remaining parameters were the same for all

repetitions. Resolution 256 × 256 pixels, field of view (FOV) 120 mm, slice thickness 3 mm, echo time (TE) 15 ms, repetition time (TR) 2000 ms, and Turbo factor 11. The total duration for 2D-IR measurements on both condyles were 10 min and 24 s. T1 was calculated pixel wise by performing a three-parameter fit of the data to a longitudinal magnetization recovery curve.

The 3D-LL sequence was implemented as described in the theory section and was used with the following parameters. Resolution 256 × 256 pixels, 30 slices, FOV 160 mm, slice thickness 3 mm, nominal FA 6°, TE 2.15 ms, TR 2500 ms, 12 contrasts (i.e., inversion times, TIs). First TI was 98 ms, and each excitation pulse was separated 4.84 ms. A hyperbolic secant pulse was used to achieve adiabatic inversion. The duration of the 3D-LL sequence was 10 min and 42 s. A few of the 3D-LL in vivo measurements were made with a FOV of 120 mm, which led to a few minor changes in the timing parameters. This was, however, of no significance to the results.

Phantom Experiments

Five glass-tubes containing Ni-doped Agarose gel (13) with different T1 and approximately equal T2 were used in the phantom experiments. T1 was measured for each tube using both 2D-IR and 3D-LL. For 2D-IR the center of the tubes was positioned through the imaging plane and for 3D-LL the tubes were positioned to extend through all acquired slices. Regions of interest (ROIs) were drawn for each tube in each acquired slice. The size of each ROI was 11 × 11 pixels. The average T1 was calculated for each ROI.

The phantom 3D-LL data were pixel-wise T1 evaluated using both the constant and the local FA correction methods. By combining the average local FA corrected T1 data and the average uncorrected T1* data for each ROI, a flip angle slice profile was calculated for each phantom, as described in the theory section.

To verify that the calculated T1 was not affected by T2-differences between the phantoms, the T2 in each phantom was previously measured using a standard two-dimensional Multiple Spin Echo (2D-MSE) sequence.

A larger phantom (length 400 mm, diameter 120 mm), containing diluted Gd-$(DTPA)^{2-}$ (Magnevist®, Scheering AG, Berlin, Germany), was used to verify the B1-independence of the local FA correction method. The phantom was large enough to extend out through both ends of the T/R coil where the B1-field becomes inhomogeneous. The 3D-LL sequence was then executed using the same parameters as above, but with the frequency encoding direction parallel to the length direction of the phantom and the FOV set to 350 mm to cover the whole phantom. A 2D-IR T1 measurement was also performed in the center of the phantom for calculation of a reference T1 value.

With this reference T1 value together with Eqs. [4, 9] the local K-value can be calculated for the Look-Locker data. Furthermore, by invoking Eq. [10], the true local FA can also be calculated. Such calculations were performed in a line profile in the length direction of the phantom, along the centerline of the coil. T1 was also calculated along the same line using the local FA correction method, with an assumed K = 1, as would be the case, for example, in the in vivo data.

In Vivo Study

A study with 33 measurement occasions (a total of 24 individuals, from which 9 were examined twice at two separate occasions) was performed. In these 33 measurement occasions, 18 were male and 15 were female, having a mean age of 45 years (standard deviation was 6 years). All subjects are from a well-described prospective cohort comprising 100 subjects who have sustained a total anterior cruciate ligament (ACL) injury in average 20 years before this study (14). From previous reports one could expect a radiographic OA rate of 60–100% in subjects 20 years after an ACL injury (15). However, subjects in this study consist of a subgroup of non ACL-reconstructed, who managed to cope with the injury, and has previously been shown to have a prevalence of tibiofemoral OA of 11% at 15 years after injury (16).

The subjects were injected with a triple-dose of Gd-$(DTPA)^{2-}$ (Magnevist®) after which the subjects were instructed to walk along a predetermined route for 10 min. The first measurement sequence was performed at 90 min after the contrast injection, in accordance with previously established dGEMRIC protocols (17). The used dose of contrast agent was selected to be consistent with our previous dGEMRIC studies, facilitating future comparisons with these data (17). Informed consent was obtained from each subject and the study was approved by the local ethics committee.

All sequences were executed consecutively without delays. First, two sets of 2D-IR sequences were performed, positioned parallel to each other through the mid sections of the lateral and medial femur condyles in the knee with expected osteoarthritis. Next, the 3D-LL sequence was performed on the same knee, using the parameters described in the *MR acquisition* section (with FOV 160 mm for 23 subjects and FOV 120 mm for 10 subjects). The 3D-LL sequence was positioned to cover both femur condyles, with the slice orientation parallel to the previously taken 2D-IR images.

Regions of interest (ROIs) in which T1 was pixel wise evaluated, were hand-drawn to cover the weight-bearing part of each femur condyle, also in accordance with previously established dGEMRIC protocols (17). Care was taken to position the ROIs equal for both the 2D-IR and the 3D-LL sequences. The size of a typical 2D-IR ROI was approximately 160 pixels and the size of a typical 3D-LL ROI (for 160 mm FOV) was approximately 110 pixels. In the 3D-LL volume, the regions of the condyles were the ROIs were drawn were typically positioned at around slice 7 and slice 23, respectively. The average T1 was calculated for each ROI.

The 3D-LL ROIs were drawn on a data set consisting of an average of all TI-images for each slice, resulting in an image with good visual contrast between the cartilage and the synovial fluid and high signal to noise ratio (Fig. 2).

The in vivo 3D-LL data were evaluated using both the constant and local FA correction methods. The 3D-LL data were also evaluated with the pre-calculated FA

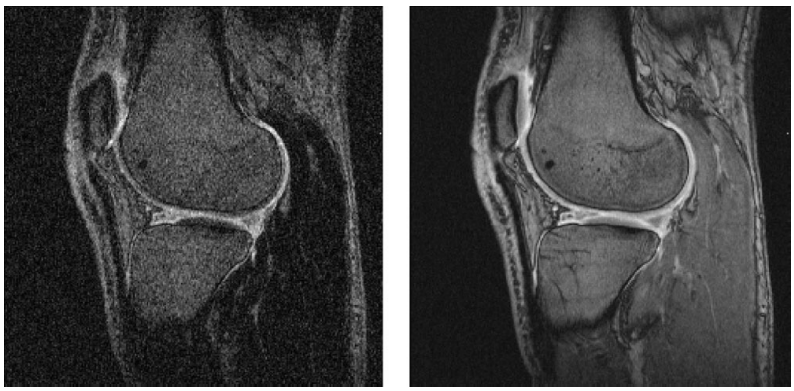

Figure 2. Image to the left is a typical raw 3D-LL TI-image. To the right is the same 3D-LL slice but shown as an average image of all TI-images for that slice. The averaged image is better suited for ROI drawing, because it has much less noise and better cartilage contrast than the raw image.

correction method, using the flip angle slice profiles from the previously measured phantoms. For this purpose an average flip angle slice profile, from the phantoms with T1 values relevant in dGEMRIC (i.e., 300 ms < T1 < 800 ms), was used.

RESULTS

Phantoms

The T1 for each of the five gel filled tubes were measured, using the 2D-IR sequence, to 196, 316, 541, 803, and 1218 ms, respectively. The corresponding T2 values were measured to 60, 64, 66, 64, and 65 ms.

Evaluation of the 3D-LL data, using the standard constant FA correction method for T1 calculation, results in a large deviation from the 2D-IR T1 values, especially in the outer slices (Fig. 3a). However, when T1 is calculated using the local FA correction method the T1 deviation from 2D-IR is less than 5% within all slices, for all T1 values relevant in dGEMRIC (i.e., 300 ms < T1 < 800 ms).

A calculation of the flip angle for different slices in the phantoms reveals the reason for the erroneous T1 values with the constant FA correction method. Due to the pulse shape of the excitation pulse, there is a severe drop in flip angle toward the outer slices (Fig. 3b), resulting in the constant FA correction method overcompensating the T1 correction in those slices. There is also a slight difference in the calculated flip angle between the different phantoms within the same slice, which might be a result of the B1-field not being in-plane homogenous. None of these flip angle variations will, however, affect the T1 calculated using the local FA correction method.

The T1 in the larger phantom was measured using 2D-IR to exactly 500 ms. In the inner part of the coil the local FA correction method also measured a constant T1 of 500 ms, but it is dropping significantly toward the ends of the coil (Fig. 4). The calculated T1 values closely follow the behavior of the K value, being constant in the inner part of the coil, but dropping toward the ends (Fig. 4). The calculated FA, however, is continuously varying,

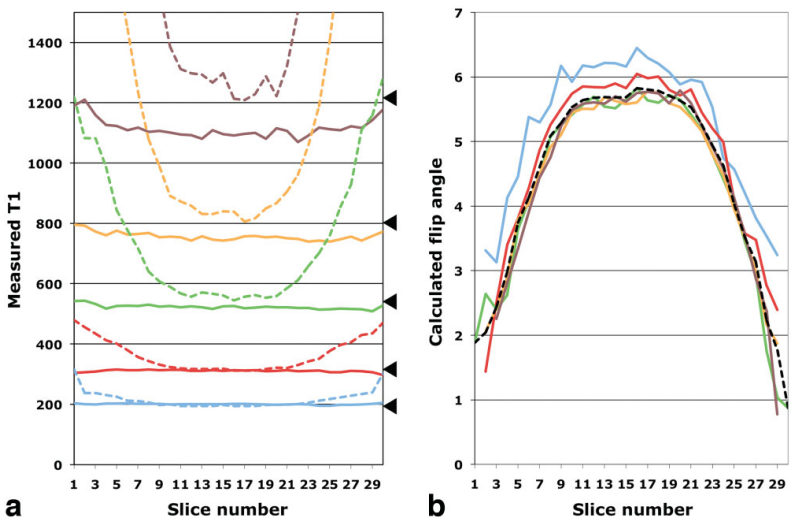

Figure 3. 3D-LL measurements for each slice in five different phantoms. **a:** Solid lines show T1 values with local FA correction. Dashed lines show T1 values with constant FA correction. Arrows to the right are T1 values for each phantom measured with 2D-IR. **b:** Calculated flip angle slice profile. The difference in flip angle between the different phantoms might be a result of the B1-field not being in-plane homogeneous. The dashed line shows the average flip angle for phantoms with T1 relevant in dGEMRIC (i.e., 300 ms < T1 < 800 ms).

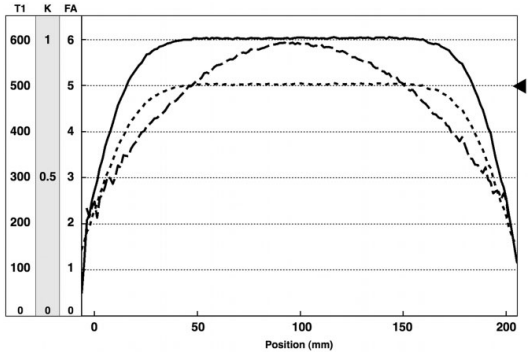

Figure 4. Evaluation of the local flip angle correction method in the presence of B1 inhomogeneities. Data represent a line profile from a large phantom extending through the full length of the T/R extremity coil. Serious B1 inhomogeneities are present as seen for the varying calculated flip angle (dashed line). The adiabatic inversion (solid line) performs good (K-value close to 1) in a large part of the phantom, but fails at the outer ends. The T1 value (dotted line) calculated with an assumed K = 1 is insensitive to the B1 inhomogeneities as long as the K = 1 assumption is true, but also fails in the outer parts where the inversion quality is poor. The arrow to the right shows reference T1 measured using 2D-IR.

reaching its nominal value only in the center of the coil (Fig. 4). This experiment thus shows that the local FA correction method results in correct T1 values regardless of the local flip angle, but at the same time is very dependent on the inversion quality.

In Vivo

T1 evaluations of both condyles were made, using each of the described methods, for all 33 subjects, resulting in a total of 66 measured ROIs for each method.

When comparing with the 2D-IR T1 values, the 3D-LL T1 values are systematically overestimated by the constant FA correction method (Fig. 5a), which is an expected result considering that the ROIs are drawn in off-center slices where the drop in flip angle is non-negligible. As can be seen, the deviation from the 2D-IR T1 values is also increasing with longer T1 for the constant FA correction method. This follows as a direct result of Eq. [2], showing that the error introduced due to overcompensating the T1 correction will increase with increased T1*.

The local FA correction method (Fig. 5b), however, seem to systematically underestimate the calculated T1 when compared with the 2D-IR T1 values. This might be a result of the inversion pulse not performing well enough in vivo. This assumption is supported by the fact that the precalculated FA correction method is performing very well in vivo (Fig. 5c).

In Table 1 the *systematic error* and the *random error* for all in vivo measurements are calculated for each of the 3D-LL evaluation methods. The systematic error is calculated as the mean of the difference between the 3D-LL T1 value and the 2D-IR T1 value for each measurement. The random error is calculated as the 95% confidence level (i.e., two times the standard deviation) for the same values. It may be noted that the random error is lowest for the local FA correction method (84.4 ms). The most accurate and precise 3D method in vivo is, however, the precalculated FA correction, resulting in both the lowest systematic error (13.3 ms) and a low random error (90.1 ms).

Table 1
Comparing In Vivo Results for the Three 3D-LL Evaluation Methods

	Constant FA correction	Local FA correction	Precalculated FA correction
Systematic error	109.1 ms	−57.5 ms	13.3 ms
Random error (95%)	127.4 ms	84.4 ms	90.1 ms

DISCUSSION

Being able to perform reliable three-dimensional dGEMRIC is an important step in the development of

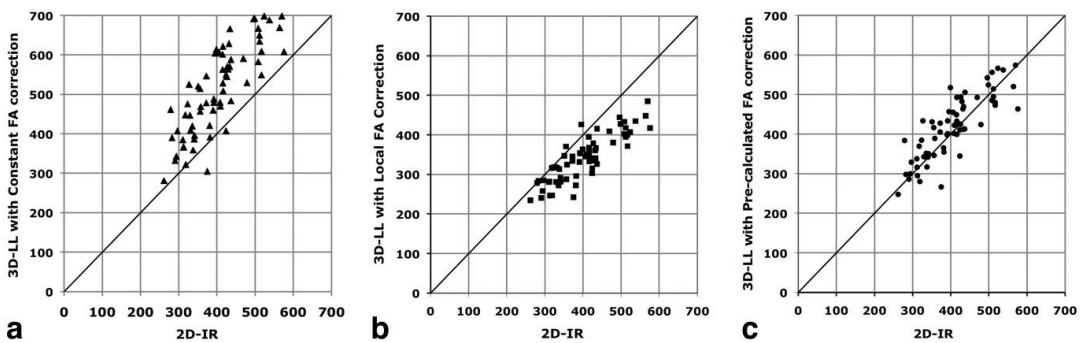

Figure 5. A total of 66 in vivo T1 measurements are made (both condyles on one knee for 33 subjects) using both 3D-LL and 2D-IR. The figures show T1 measured using 3D-LL and evaluated using each of the three evaluation methods, compared with T1 measured using 2D-IR. **a:** Constant FA correction versus 2D-IR. **b:** Local FA correction versus 2D-IR. **c:** Precalculated FA correction versus 2D-IR.

the dGEMRIC method. Not only does it enable new methods for visualization and diagnosis, but it also increases the possibilities of performing longitudinal studies. The methods presented in this study make it possible to use a larger part of the acquired volume for reliable dGEMRIC measurements, which has been a limitation with previously presented Look-Locker based methods.

Evaluating a 3D-LL sequence using the traditional constant FA correction method puts some severe restrictions on the reliability of the T1 measurements. This is mainly due to the flip angle slice profile not being perfectly rectangular, but also due to inhomogeneities in the B1-field. As is shown from the measured phantom flip angle slice profile (Fig. 3b), the actual flip angle and the nominal flip angle are only fairly equal for the centermost slices in the measured volume, for the particular pulse used in our sequence implementation. Outside of these slices there is a significant drop in flip angle, resulting in the calculated T1 being severely overestimated in these slices, which is also seen in the phantom T1 measurements (Fig. 3a).

The systematic overestimation of T1 in vivo using the 3D-LL sequence with constant FA correction is thus expected, considering that the measured ROIs are positioned at around slice 7 and slice 23, where the drop in flip angle is non-negligible. The local FA correction method presented in this study should not be sensitive to such flip angle variations. This is shown in the phantom T1 measurements where the calculated T1 is essentially constant throughout all slices with good agreement to T1 values measured using 2D-IR.

For in vivo measurements, however, the calculated T1 is somewhat underestimated with the local FA correction method. This is possibly a result of the inversion pulse not performing as well in vivo as it does in phantoms. Even though an adiabatic inversion pulse is used, it has been shown that the inversion can be nonperfect due to reasons such as the pulse amplitude or the T2 in the tissue being too low (18,19). In the equations this would be expressed by setting $K < 1$, which in turn would increase and correct the calculated T1. The large FOV phantom experiments also showed that even though the local FA correction method is insensitive to local flip angle variations from B1 inhomogeneities, it relies on a good inversion quality to give accurate results. This further supports the explanation that the underestimated T1 values in vivo can be related to poor inversion. Hence, for the local FA correction to work in vivo the local K value needs to be known (if perfect inversion cannot be assumed). Mapping the local K value would, however, require a separate method, which probably would lead to increased total scan time.

In this work, correcting the in vivo 3D-LL data with the precalculated FA correction method, using flip angle data acquired from phantom measurements, circumvents the effect of the expected nonperfect inversion. Because the calculated T1 values are shown to be correct with phantoms, the inversion apparently performs better in phantoms than in vivo. Thus, the calculated flip angle slice profile from the phantom measurements can be used to correct the in vivo data, resulting in T1 values with a very good agreement compared with the 2D-IR measurements. This approach assumes that the flip angle slice profile is similar in phantoms and in vivo, which should be the case because all sequence parameters are the same both in phantoms and in vivo. A limitation of this approach is that no consideration is taken to local B1 inhomogeneities, causing local flip angle variations, which hence still may cause errors in the calculated T1.

It may be noted that the spatial inversion quality variation for the adiabatic inversion pulse is an effect of the propagation of the RF-signal through the investigated subject. The slice dependent flip angle variation of the excitation pulse on the other hand, is an effect of the pulse bandwidth in combination with the gradient strength, which is a result of the selected sequence parameters. For this reason, it can be assumed that the excitation pulse flip angle slice profile is equal in phantoms and in vivo, while the inversion quality may differ.

The next step in development will be to further investigate how to get 3D-LL with local FA correction working in vivo. One likely approach will be to examine the possibilities of using a different inversion pulse, such as a hard non slice-selective inversion pulse, which might have a more predictable behavior. It might also be possible to use an excitation pulse with a more uniform FA slice profile, which would facilitate the T1 calculation. One such approach could be to use non slice-selective excitation pulses. This approach would, however, result in fold-in effects if the investigated object extends outside of the measured slices, and is thus limited to applications with limited size objects, such as knee-dGEMRIC. Another option could be to add an additional sequence to the protocol to simultaneously map the K value for each voxel. This would, however, increase the total acquisition time, which might pose a limitation in clinical measurements.

In theory, there could be some degree of contrast agent washout in the cartilage during the time that arises between the 2D-IR and the 3D-LL measurements. However, it has previously been shown (2,17) that the $Gd(DTPA)^{2-}$ concentration is quite constant at times between 90 and 110 min past injection, which is the timeframe in which all measurements are made. Thus, the T1 in the cartilage should be fairly constant between the different measurements.

In this study a linear phase encoding scheme was used with the 3D-LL sequence. Alternatively, it would be possible to use a centric phase encoding scheme, thus decreasing the minimum TI. However, when this was tested in phantom measurements (data not presented in this study) no difference was found in the accuracy of the measured T1 when using linear or centric encoding, for T1 values relevant in dGEMRIC.

In conclusion, a method for correction of local flip angle variations in 3D Look-Locker T1 quantification data has been presented and shown to work very well in phantom experiments. For dGEMRIC measurements in vivo the method experienced some limitations, presumably due to imperfect performance of the inversion pulse. A very good agreement with 2D-IR data could, however, be achieved also in vivo with the use of a precalculated FA correction method.

Thus it is shown that the 3D Look-Locker sequence is robust enough to perform reliable volumetric dGEMRIC measurements within clinical acceptable acquisition times. To perform such measurements it is necessary to take the flip angle slice profile into account, otherwise everything but the centermost slices must be discarded, defying the very purpose of using 3D measurements.

REFERENCES

1. Bashir A, Gray ML, Hartke J, Burstein D. Nondestructive imaging of human cartilage glycosaminoglycan concentration by MRI. Magn Reson Med 1999;41:857–865.
2. Tiderius CJ, Olsson LE, Leander P, Ekberg O, Dahlberg L. Delayed gadolinium-enhanced MRI of cartilage (dGEMRIC) in early knee osteoarthritis. Magn Reson Med 2003;49:488–492.
3. Tiderius CJ, Olsson LE, Nyquist F, Dahlberg L. Cartilage glycosaminoglycan loss in the acute phase after an anterior cruciate ligament injury: delayed gadolinium-enhanced magnetic resonance imaging of cartilage and synovial fluid analysis. Arthritis Rheum 2005;52:120–127.
4. Tiderius CJ, Svensson J, Leander P, Ola T, Dahlberg L. dGEMRIC (delayed gadolinium-enhanced MRI of cartilage) indicates adaptive capacity of human knee cartilage. Magn Reson Med 2004;51:286–290.
5. McKenzie CA, Williams A, Prasad PV, Burstein D. Three-dimensional delayed gadolinium-enhanced MRI of cartilage (dGEMRIC) at 1.5T and 3.0T. J Magn Reson Imaging 2006;24:928–933.
6. Kimelman T, Vu A, Storey P, McKenzie C, Burstein D, Prasad P. Three-dimensional T1 mapping for dGEMRIC at 3.0 T using the Look Locker method. Invest Radiol 2006;41:198–203.
7. Mamisch TC, Dudda M, Hughes T, Burstein D, Kim YJ. Comparison of delayed gadolinium enhanced MRI of cartilage (dGEMRIC) using inversion recovery and fast T1 mapping sequences. Magn Reson Med 2008;60:768–773.
8. Brix G, Schad LR, Deimling M, Lorenz WJ. Fast and precise T1 imaging using a TOMROP sequence. Magn Reson Imaging 1990;8:351–356.
9. Deoni SC. High-resolution T1 mapping of the brain at 3T with driven equilibrium single pulse observation of T1 with high-speed incorporation of RF field inhomogeneities (DESPOT1-HIFI). J Magn Reson Imaging 2007;26:1106–1111.
10. Henderson E, McKinnon G, Lee TY, Rutt BK. A fast 3D look-locker method for volumetric T1 mapping. Magn Reson Imaging 1999;17:1163–1171.
11. Look DC, Locker DR. Time saving in measurement of NMR and EPR relaxation times. Rev Sci Instrum 1970;41:250–251.
12. van der Meulen P, Groen JP, Tinus AM, Bruntink G. Fast Field Echo imaging: an overview and contrast calculations. Magn Reson Imaging 1988;6:355–368.
13. Christoffersson JO, Olsson LE, Sjoberg S. Nickel-doped agarose gel phantoms in MR imaging. Acta Radiol 1991;32:426–431.
14. Zatterstrom R, Friden T, Lindstrand A, Moritz U. Muscle training in chronic anterior cruciate ligament insufficiency—a comparative study. Scand J Rehabil Med 1992;24:91–97.
15. Lohmander LS, Englund PM, Dahl LL, Roos EM. The long-term consequence of anterior cruciate ligament and meniscus injuries: osteoarthritis. Am J Sports Med 2007;35:1756–1769.
16. Neuman P, Englund M, Kostogiannis I, Friden T, Roos H, Dahlberg LE. Prevalence of tibiofemoral osteoarthritis 15 years after nonoperative treatment of anterior cruciate ligament injury: a prospective cohort study. Am J Sports Med 2008;36:1717–1725.
17. Tiderius CJ, Olsson LE, de Verdier H, Leander P, Ekberg O, Dahlberg L. Gd-DTPA2)-enhanced MRI of femoral knee cartilage: a dose-response study in healthy volunteers. Magn Reson Med 2001;46:1067–1071.
18. Bernstein MA, King KF, Zhou XJ. Handbook of MRI pulse sequences. London: Academic Press Inc; 2004. 1040 p.
19. Kingsley PB, Ogg RJ, Reddick WE, Steen RG. Correction of errors caused by imperfect inversion pulses in MR imaging measurement of T1 relaxation times. Magn Reson Imaging 1998;16:1049–1055.

Paper II

Original Research

Repeatability of T1-Quantification in dGEMRIC for Three Different Acquisition Techniques: Two-Dimensional Inversion Recovery, Three-Dimensional Look Locker, and Three-Dimensional Variable Flip Angle

Carl Siversson, MS,[1]* Carl-Johan Tiderius, MD, PhD,[2] Paul Neuman, MD,[2] Leif Dahlberg, MD, PhD,[2] and Jonas Svensson, PhD[1]

Purpose: To evaluate the repeatability of the dGEMRIC (delayed gadolinium enhanced MRI of cartilage) method in osteoarthritis-prone knee joints for three different T1 quantification techniques: two-dimensional inversion recovery (2D-IR), three-dimensional Look-Locker (3D-LL), and three-dimensional variable flip angle (3D-VFA).

Materials and Methods: Nine subjects were examined twice, with a 2-week interval, using all three measurement techniques. Four regions of interest were defined in the central medial and lateral femoral cartilage. The repeatability was evaluated for each measurement technique. For the 3D techniques, the variation between different slices was also evaluated.

Results: Repeatability expressed by root-mean-square coefficient of variation (CV_{RMS}) showed similar results for 2D-IR and 3D-LL (5.4–8.4%). For 3D-VFA CV_{RMS} was higher (9.3–15.2%). Intraclass correlation coefficient showed both 2D-IR and 3D-LL reliability to be moderate, while 3D-VFA reliability was low. Inter-slice CV_{RMS} and ICC was of the same magnitude as the repeatability. No clear differences could be interpreted between the condyles.

Conclusion: Both 2D-IR and 3D-LL perform well in generating repeatable dGEMRIC results, while 3D-VFA results are somewhat inferior. Furthermore, repeatability results in this study are similar to previously published results for healthy subjects. Finally, the positioning of the analyzed images is crucial to generate reliable repeatability results.

Key Words: dGEMRIC; cartilage; repeatability; reproducibility; Look-Locker; variable flip angle
J. Magn. Reson. Imaging 2010;31:1203–1209.

OSTEOARTHRITIS (OA) IS a common long-term disease characterized by loss and degradation of cartilage, causing pain and dysfunction, commonly affecting the knees. In several previous studies (1–4) a method for identification of early disease related joint cartilage changes has been presented. This method, known as delayed gadolinium enhanced MRI of cartilage (dGEMRIC), provides an estimation of the glycosaminoglycan (GAG) content in the cartilage, which is shown to be decreased at early stages of OA. The technique is based on the principle that the negatively charged contrast agent $Gd(DTPA)^{2-}$ (Magnevist®, Scheering AG, Berlin, Germany), distributes in the cartilage in an inverse relationship to the GAG content. In normal cartilage, $Gd(DTPA)^{2-}$ is repelled by the abundant negatively charged GAG, whereas in conditions of GAG loss, more $Gd(DTPA)^{2-}$ will be distributed within the cartilage matrix. When the intravenously injected contrast agent has approximately reached its peak concentration in the cartilage, a quantitative measurement of T1 in the cartilage is performed, which will then correlate to the distributed amount of $Gd(DTPA)^{2-}$. Hence, longer T1 corresponds to higher cartilage quality and vice versa.

Traditionally dGEMRIC has been performed using a two dimensional T1-quantifying inversion recovery (2D-IR) sequence (1,2,4). Recently, however, several methods for performing dGEMRIC in a three-dimensional (3D) volume of interest have emerged. In the long-term, there are many advantages of using 3D sequences for dGEMRIC. With 3D, it will be possible to evaluate the whole joint cartilage, instead of just a selected cross-section as with 2D. This will make it possible both to study local changes and lesions over

[1]Department of Radiation Physics, Lund University, Malmö, Sweden.
[2]Department of Orthopedics, Lund University, Malmö, Sweden.
*Address reprint requests to: C.S., Department of Radiation Physics, Malmö University Hospital, SE-205 02 Malmö, Sweden.
E-mail: carl.siversson@med.lu.se
Received September 29, 2009; Accepted February 8, 2010.
DOI 10.1002/jmri.22159
Published online in Wiley InterScience (www.interscience.wiley.com).

larger portions of the cartilage, and also to evaluate the use of dGEMRIC in the meniscus. However, as of today, the usage of 3D techniques in dGEMRIC is still at an early stage, mainly focused around verifying the functionality as compared to 2D techniques (5–8). The two main 3D techniques that are considered for T1 quantification in dGEMRIC today are 3D-Look Locker (3D-LL) (5,7) and 3D-variable flip angle (3D-VFA) (6,8). Both are approximately as fast as the conventional 2D-IR technique, although they cover the entire joint in one measurement.

The repeatability of the dGEMRIC method is an important issue, not only to evaluate the measurement techniques themselves, but also to gain further knowledge of the processes behind the dGEMRIC method. Because there are many factors other than the GAG concentration that might affect the measured T1 in dGEMRIC, it is important to sort out to what degree the measured T1 results are persistent and to what degree they are fluctuating between measurements.

Until now, only one full study (9) and one preliminary investigation (10) have been made regarding repeatability in knee-joint dGEMRIC measurements. Both of these were using the 2D-IR technique to investigate a group of healthy subjects. Whether or not the reported repeatability results will also pertain for patients with expected OA, where other factors may affect the results, is not yet known. Furthermore, it has not been investigated what advantages or disadvantages the usage of 3D methods could have over 2D methods in terms of generating reliable and repeatable results.

The aim of this study was to investigate these issues, by measuring the dGEMRIC repeatability in vivo for a clinically relevant and common patient cohort (anterior cruciate ligament injured) that is at risk of developing OA. The measurements were performed using each of the three different dGEMRIC techniques: 2D-Inversion Recovery (2D-IR), 3D-Look Locker (3D-LL), and 3D-Variable Flip Angle (3D-VFA).

MATERIALS AND METHODS

2D Inversion Recovery

The 2D-IR T1 measurement was performed according to a previously established standard dGEMRIC protocol (1,2,4). Each 2D-IR T1-measurement consisted of six inversion recovery spin echo images acquired using different TI (50, 100, 200, 400, 800, and 1600 ms). The remaining parameters were the same for all images. Resolution 256 × 256 pixels, field of view (FOV) 120 mm, slice thickness 3 mm, echo time (TE) 15 ms, repetition time (TR) 2000 ms and Turbo factor 11. The total duration for 2D-IR measurements on both condyles (two set of 2D-IR measurements) were 10 min and 24 s. T1 was calculated pixel wise by performing a three-parameter fit of the data to the longitudinal magnetization recovery curve.

3D Look-Locker

The 3D-LL sequence used in this study is similar to the one used by Siversson et al (7), which in turn is based on the sequence described by Henderson et al (11). A slice-selective adiabatic inversion pulse is applied followed by a train of low flip angle excitation pulses to repeatedly sample the recovery of the longitudinal magnetization using a gradient echo.

Groups of successive echoes in the pulse train are encoded into separate *k*-spaces, generating several temporally separated sets of image volumes. By fitting this data pixel wise to a longitudinal relaxation curve, an apparent longitudinal relaxation time (T1*) is acquired.

The effect of the excitation pulses on the acquired T1* is then corrected for using the *precalculated FA correction method* (7). With this method the excitation pulse FA to correct for in each slice is retrieved from an FA slice profile previously acquired using phantom measurements.

The 3D-LL sequence was used with the following parameters. Resolution 256 × 256 pixels, 30 slices, FOV 160 mm, slice thickness 3 mm, TE 2.15 ms, TR 2500 ms, 12 contrasts (i.e., inversion times, TIs). First TI was 98 ms and each excitation pulse was separated 4.84 ms. A hyperbolic secant pulse was used to achieve adiabatic inversion. Nominal excitation pulse FA was 6°. The duration of the 3D-LL sequence was 10 min and 42 s.

3D Variable Flip Angle

The 3D-VFA T1 measurement technique uses two successive 3D gradient echo (3D-GRE) imaging sequences applied with different excitation pulse flip angles. For each 3D-GRE sequence, a continuous train of excitation pulses is encoding a 3D image volume. A steady-state relation will thus describe the signal level in each voxel. This level will be dependant on several parameters, including both the FA of the pulse sequence and the T1 of the tissue (12). It has been shown that from two such 3D-GRE image volumes, acquired using different flip angles, the T1 in each voxel can be extracted, given that the FA for each sequence is known (6,13).

The following 3D-VFA parameters were used in this study: resolution 256 × 256 pixels, 30 slices; field of view (FOV) 160 mm; slice thickness 3 mm; echo time (TE) 4.76 ms; repetition time (TR) 40 ms. Excitation pulse flip angles were 4.8° and 23.9°. The total duration for the 3D-VFA measurement was 5 min and 10 s.

In Vivo Study

A study was performed with nine subjects, which were examined twice using the same dGEMRIC protocol, with a 2-week interval (average 14.1 days, standard deviation 4.4 days) between the examinations. The group consisted of four male and five female subjects, having a total mean age of 45.4 years (standard deviation 5.2 years). All data were acquired on a 1.5

Tesla (T) Siemens Sonata whole-body scanner (Siemens Medical Systems, Erlangen, Germany) using a transmit-receive CP-extremity coil.

All subjects were recruited from a well-described prospective cohort comprising 100 subjects who have sustained a total anterior cruciate ligament (ACL) injury in average 20 years before this study (14). From previous reports a radiographic OA rate of 60–100% could be expected in subjects 20 years after an ACL injury (15). However, the subjects in this study consist of 9 randomly selected persons from a subgroup of 72 patients, who managed to cope with the injury without ACL-reconstruction, after early activity modification and neuromuscular rehabilitation. This subgroup has previously been shown to have a generally good knee function (16) and a radiographic prevalence of tibiofemoral OA of only 11% at 15 years after injury (17).

Hence, even though patients in this study group have a well functioning knee, with only minor occasional radiographic OA changes, they are still at risk for developing severe OA. Because the main objective of dGEMRIC is to detect early molecular cartilage matrix changes long before typical radiographic changes can be seen—such as osteophytes, joint space narrowing or definite cartilage lesions—the chosen study group is relevant from a clinical and methodological point of view.

The subjects were injected with a triple-dose of Gd-DTPA^{2-} (Magnevist®) after which the subjects were instructed to walk along a predetermined route for 10 min. The first measurement sequence was performed at 90 min after the contrast injection, in accordance with previously established dGEMRIC protocols (18). The used dose of contrast agent was selected to be consistent with previous dGEMRIC studies, facilitating future comparisons with these data (18). Informed consent was obtained from each subject and the study was approved by the local ethics committee.

All sequences were executed consecutively without delays. First two sets of 2D-IR measurements were performed, positioned parallel to each other through the mid sections of the lateral and medial femur condyles in the ACL deficient knee. Next, the 3D-LL, followed by the 3D-VFA measurements were performed on the same knee. The 3D-LL and 3D-VFA measurements were both positioned equal, covering both femur condyles, with the slice orientation approximately parallel to the previously taken 2D-IR images.

dGEMRIC Evaluation

All T1-evaluations were made using an in-house developed software package, programmed in Matlab (The Mathworks Inc, Natick, MA). Regions of interest (ROIs), in which an average T1 was calculated, were drawn to cover the anterior and posterior parts of the central lateral and central medial femur cartilage (aCLF, pCLF, aCMF, and pCMF regions) in accordance to a scheme modified from Eckstein et al (19) (Fig. 1).

The 2D-IR repeatability evaluation was straightforward with ROIs drawn on both the lateral and medial set of 2D-IR images. With the 3D sequences, appropriate slices had to be selected before ROIs being drawn. This was achieved by comparing the position of the 3D slices and the corresponding 2D-IR images, selecting the slice covering the same part of the central femur cartilage on each condyle as the corresponding 2D-IR images. The selected slices were typically around slice 7 and slice 23. For both the 3D-LL (7) and the 3D-VFA measurements, separate sets of ROIs were drawn in the respective images to exclude any effects of movement between the sequences and also to minimize any effects of contrast differences between the sequences.

Figure 1. Anterior central lateral femoral (aCLF) and posterior central lateral femoral (pCLF) cartilage regions. Anterior and posterior ends of meniscus set the regions end-points. The same boundaries apply to medial side regions.

To further investigate the impact of the slice selection on the measured T1, ROIs were also drawn on the two slices neighboring the primary selected slice for both 3D methods. This was made for the second examination in all subjects.

Statistical Analysis

To determine the repeatability of the measurements performed using the various methods, the coefficient of variation was calculated for each ROI of each subject and also for each method. The root-mean-square value of the coefficients of variation (CV_{RMS}) was then calculated in the population for each ROI with each method. CV_{RMS} values below 10% were considered as good, and values below 5% were considered as very good (9).

To further analyze the day-to-day repeatability the intraclass correlation coefficient (ICC) was calculated, representing the error free proportion of the inter-subject score. ICC values higher than 0.75 were considered to indicate good reliability, whereas values below 0.4 indicated low reliability (9). Values in between these limits were considered to show moderate reliability.

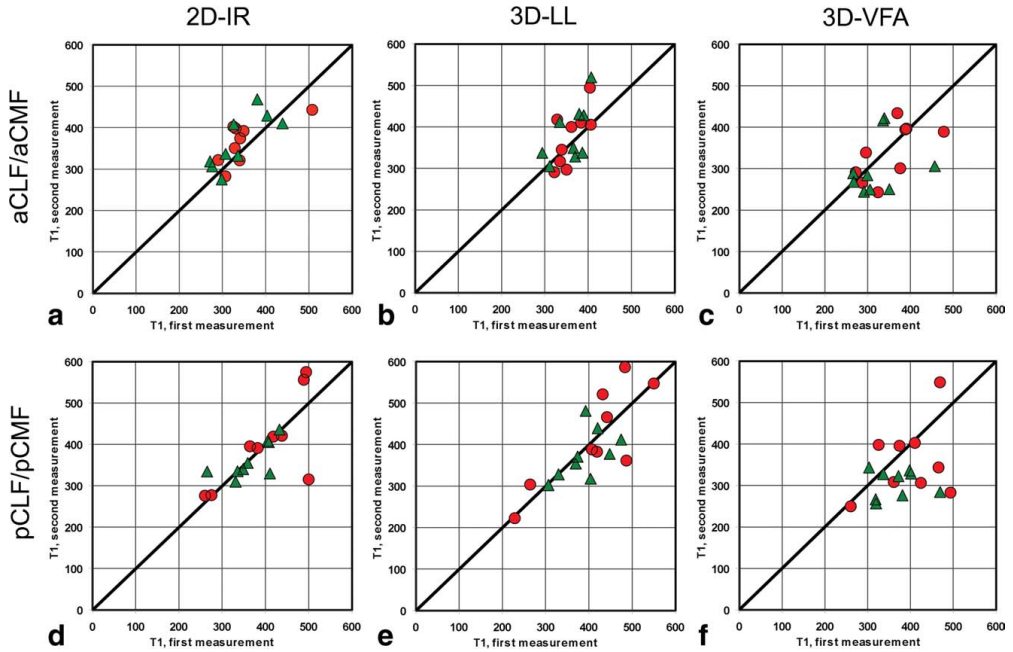

Figure 2. First and second T1 measurements in each subject. Red circles indicate lateral measurements and green triangles indicate medial measurements. **a)** aCLF and aCMF regions with 2D-IR **b)** aCLF and aCMF regions with 3D-LL **c)** aCLF and aCMF regions with 3D-VFA **d)** pCLF and pCMF regions with 2D-IR **e)** pCLF and pCMF regions with 3D-LL **f)** pCLF and pCMF regions with 3D-VFA.

For the 3D-LL and the 3D-VFA sequences, the population CV_{RMS} and ICC were also calculated to measure the inter-slice variation in T1 over the three consecutive slices where ROIs were drawn.

To verify the accuracy and the precision of the 3D sequences, the 3D-LL and 3D-VFA T1 values were also statistically compared with the corresponding values measured using 2D-IR. The Pearson correlation, the systematic error and the random error were calculated for anterior and posterior regions respectively. Systematic and random errors have previously been used in dGEMRIC for determining the accuracy of 3D T1 measurement methods (7).

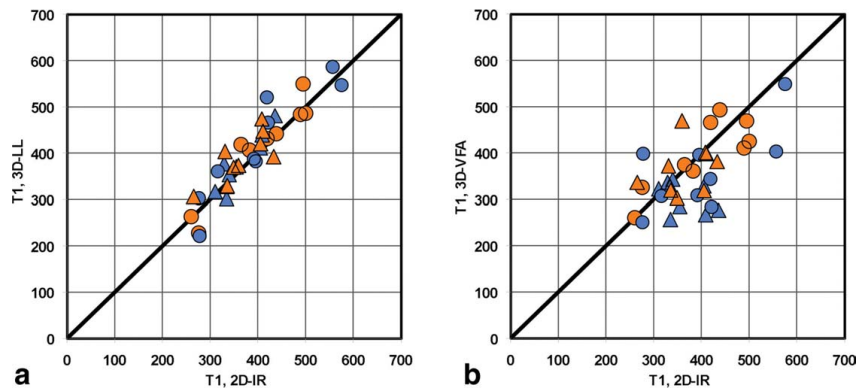

Figure 3. T1 values measured using each 3D sequence, compared with T1 values measured using 2D-IR. Circles indicate pCLF regions, and triangles indicate pCMF regions. Orange markers indicate first examination measurements and blue markers indicate second examination measurements. **a**: 3D-LL versus 2D-IR. **b**: 3D-VFA versus 2D-IR

Table 1
Measurement of repeatability (CV_{RMS} and ICC) for each T1 quantification method and for each investigated region of interest*

	aCLF	pCLF	aCMF	pCMF
2D-IR				
CV_{RMS}	**6.3**%	**8.4**%	**6.5**%	**5.4**%
ICC	0.63	0.71	0.69	0.68
T1 (ms), (SD)	356 (56)	403 (97)	351 (62)	364 (47)
3D-LL				
CV_{RMS}	**6.6**%	**7.3**%	**7.1**%	**6.5**%
ICC	0.51	0.81	0.44	0.52
T1 (ms), (SD)	367 (52)	416 (109)	371 (55)	383 (55)
3D-VFA				
CV_{RMS}	**8.0**%	**12.7**%	**11.1**%	**12.1**%
ICC	0.62	0.24	0.22	−0.34
T1 (ms), (SD)	346 (65)	379 (83)	313 (63)	336 (53)

*The average T1 values, with corresponding standard deviations, are calculated from both examinations for all subjects.

All statistical analyses were performed using custom equations solved in Excel (Microsoft, Redmond, WA).

RESULTS

Repeatability

Each T1 value, for the first and second dGEMRIC measurements are plotted, for each subject, ROI, and method, in Figure 2. All repeatability results (CV_{RMS} and ICC), together with mean T1 values, for each measurement method and for each of the analyzed regions of interest, are shown in Table 1.

For 2D-IR and 3D-LL CV_{RMS} was very similar for all ROIs, ranging between 5.4% and 8.4% with 2D-IR and between 6.5% and 7.3% with 3D-LL. With 3D-VFA CV_{RMS} was higher, ranging between 8.0% and 12.7% for the different ROIs. Thus the CV_{RMS} values for both the 2D-IR and the 3D-LL methods are good, while the CV_{RMS} values for the 3D-VFA method are somewhat inferior. Neither the 2D-IR nor the 3D-LL methods showed any clear difference in CV_{RMS}, neither between ROIs on lateral and medial condyles, nor between ROIs on the same condyle. With 3D-VFA the aCLF region stands out, showing a notably lower CV_{RMS} than the other regions (approximately 35% lower).

Particularly for the 3D-VFA method, but to some degree also for the 3D-LL method, the ICC was fluctuating heavily between the different ROIs, with a generally higher ICC for ROIs on lateral condyles. The ICC values for the 3D-VFA method were in most cases very low, ranging between −0.34 and 0.62. For 3D-LL, the ICC was higher, ranging between 0.44 and 0.81. The 2D-IR method showed a fairly constant ICC for all ROIs, ranging between 0.63 and 0.71. Thus, the ICCs for both the 2D-IR method and the 3D-LL method are indicating that the reliability of the repeatability measurements with these methods are moderate, with the 2D-IR method being slightly more reliable. The 3D-VFA method is indicating low or none reliability in these repeatability measurements, for all ROIs except the aCLF region.

Inter-slice Variation

The inter-slice variation for each region of interest, measured using both 3D T1-quantification methods, is shown in Table 2. For the 3D-LL method, CV_{RMS} is ranging between 7.3% and 13.2% in the different ROIs. The corresponding ICC is ranging between 0.65 and 0.90, showing ICC values on the medial side to be lower than those on the lateral side. For the 3D-VFA method, CV_{RMS} is ranging between 9.3% and 17.5% and the corresponding ICC is ranging between 0.32 and 0.85. CV_{RMS} values tend to be higher and ICC values tend to be lower on the medial side than the corresponding values on the lateral side.

3D Sequence Accuracy and Precision

Each pCLF and each pCMF T1 value, measured using 3D-LL and 3D-VFA, are plotted in Figure 3, against the corresponding 2D-IR T1 values. The results, together with results from anterior regions, are shown in Table 3.

Both the Pearson correlation and the random error are showing the 3D-LL measurements to be notably less scattered (i.e., higher Pearson correlation and lower random error) than the 3D-VFA measurements. This effect is most prominent in the posterior measurements, but highly notable also in the anterior measurements. The systematic error is comparable for all 3D T1 measurements, regardless of sequence or region type.

DISCUSSION

The use of a 2D-IR sequence for T1 quantification is generally considered to be a very stable method, and serves as the gold standard in this study. The measured 2D-IR repeatability is likely the best achievable of any dGEMRIC measurement method. However, in repeated dGEMRIC measurements, variations to some degree are expected, due to the complexity of both the biological and technical processes behind the measurement.

The 2D-IR and 3D-LL sequences are shown to generate roughly equally repeatable results, thus verifying the stability of the 3D-LL sequence for dGEMRIC. The results of the 3D-VFA method are less repeatable

Table 2
Measurement of inter-slice T1 variation (CV_{RMS} and ICC) for all subjects*

	aCLF	pCLF	aCMF	pCMF
3D-LL				
CV_{RMS}	7.3%	9.8%	13.2%	8.2%
ICC	0.78	0.90	0.69	0.65
3D-VFA				
CV_{RMS}	10.8%	9.3%	17.5%	12.5%
ICC	0.63	0.85	0.60	0.32

*The T1 values for all investigated regions was calculated from the second measurement for three consecutive lateral and three consecutive medial slices using each 3D T1-quantification method.

Table 3
Comparing 2D and 3D T1 results for anterior (aCLF and aCMF regions) and posterior (pCMF and pCLF regions) ROIs respectively*

	3D-LL versus 2D-IR		3D-VFA versus 2D-IR	
	Anterior	Posterior	Anterior	Posterior
Pearson correlation	0.71	0.92	0.58	0.59
Systematic error	15.5 ms	16.3 ms	−23.7 ms	−25.9 ms
Random error (95%)	85.5 ms	69.2 ms	113.5 ms	136.0 ms

*Both examinations for all subjects were included in the calculation of the results.

in this study. This might be a result of the 3D-VFA method neither taking the FA slice profile nor local FA variations into account, in combination with the method possibly being more noise sensitive than the other methods. This is also supported by the comparison in Table 3, showing that the 3D-VFA sequence generates more scattered T1 results than the 3D-LL sequence, which might be a result of such noise sensitivity in combination with local FA variations. It may be noted that because the transmit field was generated by the extremity coil, the amount of B1-inhomogeneities in these data may be more prominent than in comparable data acquired using the body coil for generating the transmit field. Early results have recently been presented (20), involving FA correction with the 3D-VFA method in dGEMRIC. By using such technique it should be possible to correct for both the effect of the FA slice profile and also the effect of other local FA variations, which might be beneficial for generating more repeatable 3D-VFA results. However, because this technique requires additional measurement sequences to be performed for calculation of a B1 map, such correction cannot be postapplied to the already acquired data presented here. It may also be noted that the 3D-VFA measurement used in this study is faster than the 3D-LL measurement. Extending the duration of the 3D-VFA measurement, for example in terms of using more than two different FAs, might improve the results.

One factor that may affect the repeatability result is the positioning of the slices, in which the ROIs are drawn, between the first and the second examination. In this study, all such positioning was based on the positioning of the 2D-IR slices, which in turn are positioned by the technologist during the examination, based on written guidelines. Thus, there is a risk of the 2D-IR slice positioning not being absolutely equal for each examination, due to both differences in patient positioning and to operator related issues. How much such slice misalignment could affect the measured T1 is approximated by the inter-slice variation analysis of the 3D sequences (Table 2), where it is seen that for a specific segment, the T1 variation (both CV_{RMS} and ICC) between the different slices is of the same magnitude as the measured repeatability for the same regions. Thus, it can be concluded that the positioning of the images is very important in a longitudinal study. A position misalignment as small as the slice thickness could cause a variation in T1 of the same magnitude as the actual repeatability of the whole method. It should be mentioned that for OA subjects, the variation between different slices is possibly higher than for healthy subjects, because the cartilage quality of OA subjects might be more inhomogeneous.

In general for the 3D methods, both the repeatability values and the inter-slice variation is slightly better on the lateral side than on the medial side. This might be an effect of the lateral side ROIs generally containing more pixels, due to the cartilage thickness, resulting in a more stable average T1 for lateral ROIs. Because a smaller voxel size was used in the 2D measurements than in the 3D measurements, this effect may not be so obvious for the 2D results. However, the difference between lateral and medial measurement results is generally too small to draw any extensive conclusions.

It is of interest to point out the low ICC for the pCLF, aCMF and pCMF regions in the 3D-VFA repeatability measurement. Such low ICC values actually suggest that the reliability of any measured repeatability is close to none. For this reason, it is remarkable that the 3D-VFA ICC value for the aCLF region is well within the range of moderate reliability.

It may be argued that there could be some degree of contrast agent washout in the cartilage during the time that arises between the 2D-IR and the 3D-VFA measurements. However, it has previously been shown (2,18) that the $Gd(DTPA)^{2-}$ concentration is relatively constant at times between 90 and 120 min past injection, which is the timeframe in which all measurements are made (total duration 26 min 16 s). Thus, the T1 in the cartilage should be fairly constant between the different measurements.

To our knowledge, only one extensive repeatability study has previously been made in the field of knee-dGEMRIC (Multanen et al)(9). In that study, the lateral condyle repeatability was measured for healthy subjects using the 2D-IR method. Multanen et al reported CV_{RMS} values of 7.1% and 4.8% for aCLF and pCLF regions, respectively. In the present study, the corresponding 2D-IR CV_{RMS} values are 6.3% and 8.4%. Similarly, Multanen et al reported ICC values of 0.80 and 0.81 for the aCLF and pCLF regions, whereas the present study reported corresponding 2D-IR values of 0.63 and 0.71. Hence, both studies are reporting approximately similar results, which is encouraging, given the relatively small number of investigated subjects in each study and also given a few technical differences in the protocols of the two studies. Thus, it can be concluded that the repeatability for dGEMRIC measurements is not affected severely between healthy subjects and patients such as those investigated in the present study.

Future improvement in repeatability would include identification of the cartilage area of interest only from landmarks within the 3D sequences. In such a case, the technologist would only have to make sure that the entire joint is covered in the measurement, and the actual area where the T1 measurement is made is identified later within the 3D volume. This would exclude the possible error factor of the slices being misaligned between the first and the second measurement as the exact same cartilage volume could always be identified within each 3D data set.

In conclusion, it is shown that both the 2D-IR and the 3D-LL methods perform well in generating repeatable dGEMRIC results, while the 3D-VFA method yield results that are somewhat inferior to the results of the two other methods. Furthermore, it is shown that that the 2D-IR dGEMRIC repeatability for ACL-deficient patients at risk of developing OA is approximately the same as previously reported repeatability results for healthy subjects. Finally, it is also concluded that the positioning of the images is crucial to generate reliable results in longitudinal studies.

REFERENCES

1. Bashir A, Gray ML, Hartke J, Burstein D. Nondestructive imaging of human cartilage glycosaminoglycan concentration by MRI. Magn Reson Med 1999;41:857–865.
2. Tiderius CJ, Olsson LE, Leander P, Ekberg O, Dahlberg L. Delayed gadolinium-enhanced MRI of cartilage (dGEMRIC) in early knee osteoarthritis. Magn Reson Med 2003;49:488–492.
3. Tiderius CJ, Olsson LE, Nyquist F, Dahlberg L. Cartilage glycosaminoglycan loss in the acute phase after an anterior cruciate ligament injury: delayed gadolinium-enhanced magnetic resonance imaging of cartilage and synovial fluid analysis. Arthritis Rheum 2005;52:120–127.
4. Tiderius CJ, Svensson J, Leander P, Ola T, Dahlberg L. dGEMRIC (delayed gadolinium-enhanced MRI of cartilage) indicates adaptive capacity of human knee cartilage. Magn Reson Med 2004;51:286–290.
5. Li W, Scheidegger R, Wu Y, Vu A, Prasad PV. Accuracy of T1 measurement with 3-D Look-Locker technique for dGEMRIC. J Magn Reson Imaging 2008;27:678–682.
6. Mamisch TC, Dudda M, Hughes T, Burstein D, Kim YJ. Comparison of delayed gadolinium enhanced MRI of cartilage (dGEMRIC) using inversion recovery and fast T1 mapping sequences. Magn Reson Med 2008;60:768–773.
7. Siversson C, Tiderius CJ, Dahlberg L, Svensson J. Local flip angle correction for improved volume T1-quantification in 3D dGEMRIC using the Look-Locker technique. J Magn Reson Imaging 2009;30:834–841.
8. Trattnig S, Marlovits S, Gebetsroither S, et al. Three-dimensional delayed gadolinium-enhanced MRI of cartilage (dGEMRIC) for in vivo evaluation of reparative cartilage after matrix-associated autologous chondrocyte transplantation at 3.0T: preliminary results. J Magn Reson Imaging 2007;26:974–982.
9. Multanen J, Rauvala E, Lammentausta E, et al. Reproducibility of imaging human knee cartilage by delayed gadolinium-enhanced MRI of cartilage (dGEMRIC) at 1.5 Tesla. Osteoarthritis Cartilage 2009;17:559–564.
10. Burstein D, Velyvis J, Scott KT, et al. Protocol issues for delayed Gd(DTPA)(2-)-enhanced MRI (dGEMRIC) for clinical evaluation of articular cartilage. Magn Reson Med 2001;45:36–41.
11. Henderson E, McKinnon G, Lee TY, Rutt BK. A fast 3D look-locker method for volumetric T1 mapping. Magn Reson Imaging 1999;17:1163–1171.
12. van der Meulen P, Groen JP, Tinus AM, Bruntink G. Fast field echo imaging: an overview and contrast calculations. Magn Reson Imaging 1988;6:355–368.
13. Wang HZ, Riederer SJ, Lee JN. Optimizing the precision in T1 relaxation estimation using limited flip angles. Magn Reson Med 1987;5:399–416.
14. Zatterstrom R, Friden T, Lindstrand A, Moritz U. Muscle training in chronic anterior cruciate ligament insufficiency--a comparative study. Scand J Rehabil Med 1992;24:91–97.
15. Lohmander LS, Englund PM, Dahl LL, Roos EM. The long-term consequence of anterior cruciate ligament and meniscus injuries: osteoarthritis. Am J Sports Med 2007;35:1756–1769.
16. Kostogiannis I, Ageberg E, Neuman P, Dahlberg L, Friden T, Roos H. Activity level and subjective knee function 15 years after anterior cruciate ligament injury: a prospective, longitudinal study of nonreconstructed patients. Am J Sports Med 2007;35:1135–1143.
17. Neuman P, Englund M, Kostogiannis I, Friden T, Roos H, Dahlberg LE. Prevalence of tibiofemoral osteoarthritis 15 years after nonoperative treatment of anterior cruciate ligament injury: a prospective cohort study. Am J Sports Med 2008;36:1717–1725.
18. Tiderius CJ, Olsson LE, de Verdier H, Leander P, Ekberg O, Dahlberg L. Gd-DTPA2- enhanced MRI of femoral knee cartilage: a dose-response study in healthy volunteers. Magn Reson Med 2001;46:1067–1071.
19. Eckstein F, Ateshian G, Burgkart R, et al. Proposal for a nomenclature for magnetic resonance imaging based measures of articular cartilage in osteoarthritis. Osteoarthritis Cartilage 2006;14:974–983.
20. Andreisek G, White LM, Yang Y, Robinson E, Cheng HL, Sussman MS. Delayed gadolinium-enhanced MR imaging of articular cartilage: three-dimensional T1 mapping with variable flip angles and B1 correction. Radiology 2009;252:865–873.

Paper III

[redacted]

Since this paper is not yet published it has been removed from the public online version of this thesis. The full version of the thesis is available upon request. Please send an email to carl.siversson@med.lu.se

Paper IV

[redacted]

Since this paper is not yet published it has been removed from the public online version of this thesis. The full version of the thesis is available upon request. Please send an email to carl.siversson@med.lu.se

LUND UNIVERSITY

Lund University, Faculty of Medicine Doctoral Dissertation Series 2011:74
ISBN 978-91-86871-24-6
ISSN 1652-8220
Printed in Sweden by Media-Tryck, Lund 2011